Studies of optical properties of lanthanide upconversion nanoparticles for emerging applications

Qingyun Liu

Doctoral Thesis in Theoretical Chemistry and Biology
School of Engineering Sciences in Chemistry, Biotechnology and Health
Royal Institute of Technology
Stockholm, Sweden 2020

ISBN 978-91-7873-500-6
TRITA-CBH-FOU-2020:18
Printed by Universitetsservice US-AB,
Stockholm, Sweden, 2020
Typeset in LaTeX by the research group of Prof. Hans Ågren.

To my past PhD student life

Abstract

YTTERBY, a small village very close to Stockholm where I live, is the place in the world which has lent its name to the largest number of elements in the periodic table, namely four - YTTRIUM, YTTERBIUM, ERBIUM and TERBIUM. Three more lanthanide elements were discovered from the now empty quarry located in this village. By the time of their discoveries in the 19th century little could be known about their fantastic properties, the versatility of their use and functionality in what we now call nanotechnology. This is a circumstance that motivated me to rather recently enter lanthanide research, in particular studies of their outstanding optical properties for the purpose of information technology and energy harvesting.

So far, upconversion nanoparticles (UCNPs) have been much explored as unique spectral converters for various applications, like biotechnology, information technology and photovoltaic devices due to properties like sharp emission profiles, low autofluorescence and large anti-Stoke shifts. Still, there is much to explore and to understand in order to fully utilize the very unique properties of UCNPs. The kinetic dynamics of the upconversion process is one such aspect that is not well understood, and a deeper understanding of the kinetic dynamics of lanthanide upconversion systems could thus broaden their applications. Therefore, the work of this thesis is focused on investigating the kinetic dynamics of upconversion processes mainly based on systems with $NaYF_4$ as host material, and Yb^{3+}/Er^{3+} or Yb^{3+}/Tm^{3+} embedded as sensitizer/activator. Through rate equation models, the kinetic dynamics of upconversion are comparatively investigated with numerical simulations and analytical derivation. The temporal response regarding upconverted luminescence and quantum yield power density dependence, excitation duration response and excitation frequency response of the upconversion systems are investigated and the corresponding applications for multicolor imaging, optical encoding, photovoltaics, IR photodetectors are explored and analyzed in the thesis, taking advantage of the kinetic properties.

Sammanfattning

YTTERBY, en liten by nära Stockholm där jag bor, är den plats i världen som har lånat sitt namn till det högsta antalet element i det periodiska systemet, nämligen fyra - YTTRIUM, YTTERBIUM, ERBIUM och TERBIUM. Ytterligare tre lantanidelement upptäcktes från det nu tomma stenbrottet som ligger i denna by. Vid deras upptäckter på 1800-talet kunde man inte ana deras fantastiska egenskaper, mångsidigheten i deras användning och deras funktionalitet i det vi nu kallar nanoteknologi. Detta är en omständighet som motiverade mig ganska nyligen att intressera mig för lantanidforskning, i synnerhet studier av deras enastående optiska egenskaper och deras energitillämpningar och användning inom informationsteknik.

Hittills har uppkonverterande nanopartiklar (UCNPs) utforskats mycket som unika spektralkonverterare för olika applikationer, som bioteknik, informationsteknologi och fotovoltaiska enheter på grund deras egenskaper som skarpa emissions profiler, låg autofluorescens och stora anti-Stoke skift. Det finns fortfarande mycket att utforska och förstå för att utnyttja de mycket unika egenskaperna hos dessa partiklar. Den kinetiska dynamiken i upkonverteringsprocessen är en sådan aspekt som inte är väl undersökt ännu, och en djupare förståelse av den kinetiska dynamiken i uppkonverterande lantanid system kan bredda deras tillämpningar. Därför har jag fokuserat arbetet med den här avhandlingen på att undersöka den kinetiska dynamiken i upkonverterings processen huvudsakligen baserat på system med $NaYF_4$ som värdmaterial och Yb^{3+}/Er^{3+} eller Yb^{3+}/Tm^{3+} inbäddat som sensibilisator/aktivator. Genom simuleringar av ekvationsmodeller har jag undersökt den kinetiska dynamiken i uppkonversionen jämförande numerisk simulering och analytisk härledning. Det temporära svaret med avseende på uppkonverterad luminescens, det s.k. täthetsberoendet av kvantutbytet och excitation frekvens responsen för olika upkonversionssystem har studerats. Motsvarande tillämpningar för flerfärgs avbildning, optisk kodning, fotovoltaik och IR fotodetektorer undersöks och analyseras i avhandlingen, med speciell fokus på de kinetiska egenskaperna.

Abbreviations

QDs	Quantum dots
NPs	Nanoparticles
UC	Upconversion
UCNPs	Upconversion nanoparticles
PL	Photoluminescence
UCL	Upconversion luminescence
Ln	Lanthanide
QY	Quantum yield
NIR	Near infrared
IR	Infrared
UV	Ultraviolet
Vis	Visible
CW	Continuous wave
CIE	Commission international de l'éclairage
GSA	Ground state absorption
ESA	Excited state absorption
ETU	Energy transfer upconversion
CR	Cross relaxation
PA	Photon avalanche
RE	Rare earth
MPR	Multiphonon relaxation
NRs	Nanorods
IRF	Impulse response function
DSSCs	Dye sensitized solar cells
MLA	Microlens array
EM	Electromagnetic
J_{sc}	Short-circuit current density
V_{oc}	Open-circuit voltage
FF	Fill factor
η	The overall efficiency of solar cells
J-V	Current density-voltage
λ	Wavelength of light
TEM	Transmission electron microscopy
SEM	Scanning electron microscopy

Preface

The work was carried out at the Division of Theoretical Chemistry and Biology, School of Engineering Sciences in Chemistry, Biotechnology and Health, Royal Institute of Technology (KTH), Sweden.

List of papers included in the thesis

Paper I Niusha Bagheri, **Qingyun Liu**, Jan Bergstrand, Rui Pu, Qiuqiang Zhan, Mohammad Hossein Majles Ara, Hans Ågren, Haichun Liu, Jerker Widengren.

Change in the emission saturation and kinetics of upconversion nanoparticles under different light irradiations. *Optical Materials*, 2019, 97, 109389.

Paper II Jan Bergstrand, **Qingyun Liu**, Bingru Huang, Xingyun Peng, Christian Wurth, Ute Resch-Genger, Qiuqiang Zhan, Jerker Widengren, Hans Ågren and Haichun Liu.

On the decay time of upconversion luminescence.*Nanoscale*, 2019, 11, 4959-4969.

Paper III **Qingyun Liu**, Haichun Liu, Deyang Li, Wen Qiao, Guanying Chen and Hans Ågren.

Microlens array enhanced upconversion luminescence at low excitation irradiance. *Nanoscale*, 2019, 11, 14070-14078.

Paper IV Yanan Ji, Wen Xu, Nan Ding, Haitao Yang, Hongwei Song, **Qingyun Liu**, Hans Ågren, Jerker Widengren, Haichun Liu.

Cascade photon upconversion amplification for selective multispectral narrow-band near-infrared photodetection. Submitted manuscript.

Paper V **Qingyun Liu**, Lucía Labrador-Páez, Jan Bergstrand, Xiang Zheng, Yong Zhang, Jerker Widengren, Haichun Liu, Hans Ågren.

High throughput decoding approach for luminescence kinetics-based optical encoding of lanthanide upconversion nanoparticles. Manuscript under edition.

Comments on my contribution to the papers included

As the first author of the included papers, I took major responsibility for the experiments, analysis and writing of the Papers I, III and V.

As co-author, I took partial responsibility for experiments, analysis of data or discussion in Papers II, IV.

List of papers not included in the thesis

Paper I Asghar Jamshidi Zavaraki, **Qingyun Liu**, Hans Ågren.

Solar cell sensitized with "green" InP-ZnS quantum dots: Effect of ZnS shell deposition. Nano-Structures & Nano-Objects, 2020, 22, 100461.

Acknowledgments

I would like to express my sincere acknowledgments to the people who have helped me during my doctoral study.

First of all, I would like to give my deep gratitude to my supervisor Hans Ågren and my co-supervisor Haichun Liu. Thank you for all the freedom, Hans, you provided for my research. Haichun is always patient and taught me a lot and guided me through all my projects. His rigorous scientific research spirit helped me to build a better scientific methodology and scientific morality.

Many thanks to Prof. Jerker Widengren for providing great optical experimental environment and the guidance.

Many thanks to Prof. Patrick Norman for providing the wonderful working environment, Prof. Yaoquan Tu for his kind help, especially with the eISP and truly thanks to Nina Bauer, who has already left the department to enjoy her retired time, to help me with administrative process and I miss her sarcastic humor.

I would like to thank Prof. Faris Gelmukhanov, Prof. Olav Vahtras, Prof. Mårten Ahlquist, Prof. Zivinas Rinkevicius, Prof. Yi Luo, Dr. Xin Li, Dr. Viktor Kimberg and Dr. Mathieu Linares for either the lectures, seminars or speeches in the department, for the part I am able to understand as an experimentalist.

I sincerely appreciate the good company of my good friends&colleagues in the department of TCB: Dr. Zhen Xie, Karan Noori Ahmadzadeh, Manuel Brand, Juan Angel De Gracia Triviño, Dr. Camilla Gustafsson, Dr. Michal Biler, Xiaoyu Chen, Dusanka Golo, Junhao Li, Yogesh Todarwal, Viktoriia Savchenko, Dr. ShaoQi Zhan, Yang Zhou, Ge Li, Dr. Pooria Farahani, Dr. Lucía Labrador, Dr. Uliana Kostiv, Dr. Guanglin Kuang, Dr. Magnus Ringholm, Dr. Hao Su, Dr. Rafael Carvalho Couto, Dr. Markéta Paloncyova, Dr. Reza Zarei, Dr. Xu Wang, Dr. Vinícius Vaz da Cruz, Dr. Nina Ignatova, Dr. Iulia Brumboiu, Dr. Jing Huang, Dr. Gleb Baryshnikov, Dr. Vadim Zakomirnyi, Dr. Dirk Rehn, Yuya Yamaura, Dr. Haofan Sun, Dr. Rong-Feng Zou, Dr. Tobias Fahleson, Dr. Michal Biler, Dr. Nanna Holmgaard List, Dr. Asghar Jamshidi Zavaraki, Dr. Balamurugan.

Among them, with extra thanks to my lunch pals for the amazing deep philosophical talk, good laugh and great company over lunch, which consists of big part of my limited daily social life.

I sincerely appreciate the assistance of my colleagues in the department of Applied physics: Niusha Bagheri, Joachim Piguet, Elin Sandberg, Baris Demirbay, Dr. Jan Bergstrand.

I would like to thank the China Scholarship Council (CSC) for the financial support for my PhD studies in Sweden.

Special thanks to my friends Tong Han and Yang Wang, for their 4 years' companionship through my PhD study in Sweden and the tasty well cooked food.

Special thanks to my dear friend Alexander John Lind, for his incredible patience, support and company when I was very down and struggled with my PhD life and for opening my mind, expanding my horizons endlessly with his unimaginable deep philosophical questions and thoughts, which I struggled to even understand.

At last, I would like to express my deepest thanks to my parents, my sisters and all other family members, for their selfless care, unconditional love and patience.

CONTENTS

Chapter 1

Introduction

1.1 Nanotechnology

Few scientific endeavors have transformed our perception of nature like the development of nanotechnology. This is a technology by which matter at the nanoscale, of the range 1-100 nm, is manipulated, and is utilized in the design, characterization, production and application of materials, structures, devices and systems. Materials structured at the nanoscale possess unique physiochemical attributes and provide unprecedented capabilities that nowadays are exploited in many important societal areas. Its wide applications involving production of new materials have changed people's life significantly in many aspects in the last quarter of a century, like for the use of healthcare systems,[1] clean energy technology,[2] and information technology.[3] The academic and industry sectors are both embracing nanotechnology. Due to their size range, the materials within the nanoscale exhibit properties which can not be seen for bulk sizes.

The success of nanotechnology can essentially be traced to two outstanding properties of nanoparticles: quantum confinement, leading to discrete energy states (*e.g.*, quantum dots (QDs)),[4] and the ability to support collective electron oscillations (*e.g.*, plasmons).[5] In recent years, upconversion nanoparticles (UCNPs) have attracted increasing attention for upconversion lasers,[6] photovoltaic devices,[7] photocatalysis,[8] biological sensing,[9] optical encoding[10] and labeling.[11] Compared with traditional single-photon-excited fluorescence materials, such as semiconductor QDs and organic fluorophores, upconversion luminescence (UCL) materials exhibit numerous advantages for the potential applications mentioned above, including high sensitivity, weak background autofluorescence, resistance to photodestruction, low toxicity, large anti-Stokes shifts, low-cost fabrication, relatively high chemical stability, etc. Following all the advantages of UCNPs, various scientific

fields have witnessed a tremendous development, like nanochemistry, including sophisticated size,[12] phase,[11] structure[13] and morphology manipulation[14] of UCNPs with high precision, and surface modification[12] with specific applications purpose.

1.2 Motivations of this thesis research

In this thesis I emphasize a dimension of nanotechnology that recently has emerged, namely the ability of specifically designed nanoparticles to selectively convert incident light into other spectral regions. One can design lanthanide doped nanoparticles that can either efficiently down-convert the harvested light excitation energy, manifesting intense multiple peaks of photoluminescence emission at longer wavelengths, or up-convert the light energy, involving sequential or step-wise absorption of two or more excitation photons via intermediate long-lived electronic states, to produce higher energy photons at near infrared (NIR), visible (Vis) or ultraviolet (UV) range. These nanoparticles can be efficiently excited in the NIR at low excitation power that promotes their use in optical bioapplications,[15] information technology,[10,16] and light harvesting for photovoltaic devices.[17,18] My studies concern advancing experimentation to control light and energy transfer in lanthanide doped nanoparticles, explore their optical response and the corresponding applications. The results I have obtained in this area are reported in this thesis. The goal of this thesis is thus to advance the research for the purpose of controlling the optical properties of lanthanide UCNPs and to study the optical dependence of their spectral response. My wish is that my research work can inspire other researchers to deeply investigate UCNPs: optical properties and their emerging applications.

Chapter 2

Lanthanide-doped Upconversion nanoparticles

2.1 Lanthanides

Lanthanides (Lns) were first discovered in a black, heavy, mineral in the Ytterby village in Sweden by Carl Axel Arrhenius in 1787, and the elements ytterbium, yttrium, erbium and terbium were named after this village later on. With time, various lanthanide elements were separated from this mineral Gadolinnite. Seven years later after the first discovery of lanthanides, the Finnish chemist Johan Gadolin obtained yttria from the mineral, the first rare earth (RE) compound containing yttrium. Berzelius and, independently, Klaproth discovered the RE compound cerite, containing the element cerium in the same year 1803 but in two different countries (one in Sweden and one in Germany). Since many lanthanides are contained in the same mineral, it was very challenging for the nineteenth century chemists to separate them due to their similar properties. Later on, with the invention of the spectroscope, the English physicist Henry Moseley was able to demonstrate that there are 15 lanthanide elements in total, from lanthanum to lutetium. Due to that their appearance is limited to relatively rare mines, they are named rare earth elements, in spite of fact that these elements are relatively plentiful in Earth's crust, except promethium.

The lanthanides comprise 15 chemical elements with atomic number ranging from 57 to 71 (La, Ce, Pr, Nd, Pm, Sm, Eu, Gd, Tb, Dy, Ho, Er, Tm, Yb, Lu). Together with the elements scandium (Sc) and yttrium (Y) they are categorized together as rare earth elements. All these elements can form trivalent cations and the +3 oxidation state is dominating, *i.e.*, RE^{3+}(Sc^{3+}, Y^{3+}, La^{3+}, Ce^{3+}, Pr^{3+}, Nd^{3+}, Pm^{3+}, Sm^{3+}, Eu^{3+}, Gd^{3+}, Tb^{3+}, Dy^{3+}, Ho^{3+}, Er^{3+}, Tm^{3+}, Yb^{3+} and Lu^{3+}). Except La, the lanthanides are f-block elements, referring to the filling of the $4f$ orbitals. The lanthanides share some similar properties, like that the coordination number is greater than 6 (usually 8-9) when they appear in compounds,[19] and a

.

Table 2.1: *Electronic configuration of lanthanide elements and their corresponding Ln^{3+}.*

Element	Symbol	Electronic configuration	Configuration Ln^{3+}
lanthanum	La	[Xe]$4f^0 5d^1 6s^2$	[Xe]$4f^0$
cerium	Ce	[Xe]$4f^1 5d^1 6s^2$	[Xe]$4f^1$
praseodymium	Pr	[Xe]$4f^3 5d^0 6s^2$	[Xe]$4f^2$
neodymium	Nd	[Xe]$4f^4 5d^0 6s^2$	[Xe]$4f^3$
promethium	Pm	[Xe]$4f^5 5d^0 6s^2$	[Xe]$4f^4$
samarium	Sm	[Xe]$4f^6 5d^0 6s^2$	[Xe]$4f^5$
europium	Eu	[Xe]$4f^7 5d^0 6s^2$	[Xe]$4f^6$
gadolinium	Gd	[Xe]$4f^7 5d^1 6s^2$	[Xe]$4f^7$
terbium	Td	[Xe]$4f^9 5d^0 6s^2$	[Xe]$4f^8$
dysprosium	Dy	[Xe]$4f^{10} 5d^0 6s^2$	[Xe]$4f^9$
holmium	Ho	[Xe]$4f^{11} 5d^0 6s^2$	[Xe]$4f^{10}$
erbium	Er	[Xe]$4f^{12} 5d^0 6s^2$	[Xe]$4f^{11}$
thulium	Tm	[Xe]$4f^{13} 5d^0 6s^2$	[Xe]$4f^{12}$
ytterbium	Yb	[Xe]$4f^{14} 5d^0 6s^2$	[Xe]$4f^{13}$
lutetium	Lu	[Xe]$4f^{14} 5d^1 6s^2$	[Xe]$4f^{14}$

preference to bond to more electronegative elements (*e.g.*, O, F). The electronic configuration of Ln^{3+} can be represented as [Xe] $4f^x 5d^y 6s^2$, where x ranges from 0 to 14, and y ranges from 0 to 1. The electron configuration of all lanthanides elements are shown in table 2.1.

Due to the shielding effect of the outside electrons $5s$, $5p$ and $6s$, the $4f$ orbitals penetrate the core [Xe] and are isolated from forming chemical bonding, making them relatively stable and with small interaction with environmental crystal fields.[20,21] As a result, the photoluminescence emission profiles of $4f$ orbitals are very sharp, which is beneficial for applications like information technology and bioimaging. Not all lanthanide elements are photoluminescent, as shown by the energy level structure of the lanthanide ions in Fig. 2.1. The lanthanide elements, Yb^{3+}, Ce^{3+} and Gd^{3+} have simple energy level structure, and elements: Pr^{3+}, Nd^{3+}, Sm^{3+}, Eu^{3+}, Tb^{3+}, Dy^{3+}, Ho^{3+}, Er^{3+} and Tm^{3+} are luminescent.

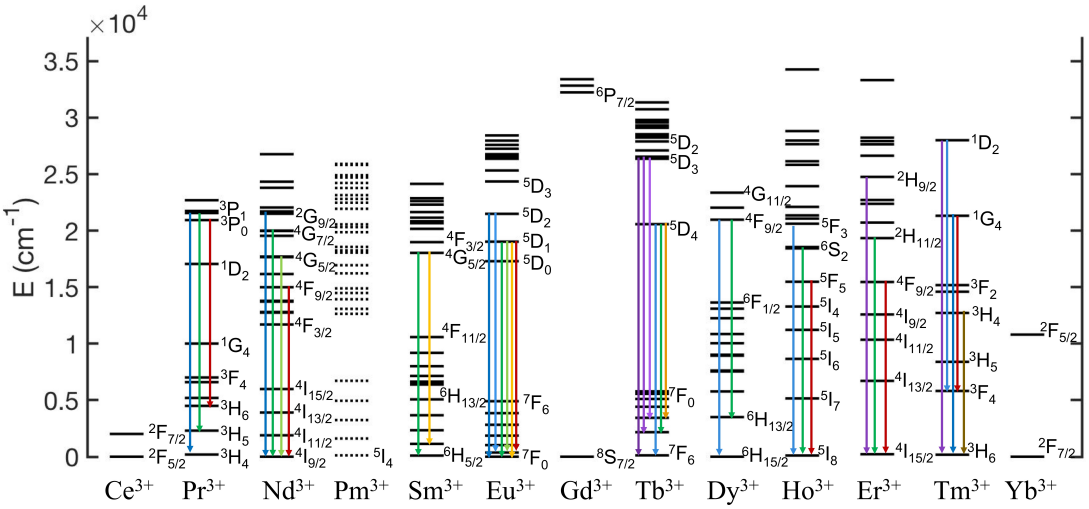

Figure 2.1: *Partial energy diagram of commonly used upconversion lanthanide ions.*

2.2 Lanthanide-doped upcoversion nanoparticles

Upconversion nanoparticles (UCNPs) mostly consist of lanthanide-doped dielectric nanomaterials whereby lanthanide ions are diluted in an appropriate inorganic host lattice with a dimension of usually less than 100 nm. The involvement of real intermediate energy levels enables light upconversion to be efficiently produced with an excitation power density as low as $\sim 10^{-1}$ W/cm^2, easily provided by low-cost commercialized laser diodes or bulb lamps. This is in remarkable contrast to the high power density excitation ($> 10^6$ W/cm^2) required in nonlinear multi-photon absorption or second harmonic generation. Moreover, the wave functions involved in their $4f$-$4f$ electronic transitions are well localized within a single ion. As a consequence, upconversion nanoparticles do not exhibit quantum confinement effects that are clearly manifested in semiconducting materials, and show luminescence that is quite stable in varying environments with line-like sharp emissions and exhibit high resistance to photobleaching and photochemical degradation. By a judicious selection of one or more lanthanide dopants, upconverted luminescence can be generated at a number of selective wavelengths (*e.g.*, 409 nm, 450 nm, 525/540 nm, 654 nn), to allow for multiplexed color emission.[22]

While there nowadays is substantial flexibility in the design of UCNPs, there are some fundamental rules to follow. UCNPs contain three appropriate components: host material, activator (UCL center) and sensitizer (to harvest energy). Some

considerations should be followed for determining good potential candidates. For choosing an appropriate host material, properties of optically transparency in the spectra range of interest and chemical and optical stability should be considered first. Except that, the phonon dynamics and the local crystal field of the host material should be taken into consideration. High value of maximal phonon energy (cutoff phonon energy) could lead to strong undesired nonradiative depopulation of the UCL states. At the same time, host phonon energy can assist energy transfer between energy mismatching states. The balance between the two effects should be considered carefully when choosing appropriate host material. The local crystal field of the host material can have a profound effect on the UCL efficiency since it has a significant influence on the optical properties to determine the spectral position, energy splitting of dopant ions and dopant ion distance. In general, host materials with low symmetry are preferred to favor $4f$-$4f$ transitions. Moreover, the crystal structure lattice should match with the dopant ions radius.[23] Taking these facts into consideration, fluorides ($NaYF_4$, with cutoff phonon energy $\sim$350 cm^{-1}) are considered to be good host material candidates and have so been well investigated.[24,25] To chose appropriate sensitizer ions, factors of simple energy level structure, relatively long excited state lifetime, big absorption cross-section and matching of excitation wavelength with commercial available laser diodes should be taken into account. Because of the above mentioned factors, Yb^{3+} and Nd^{3+} have been well explored as sensitizers. For activators, ions should be luminescent with relatively abundant energy level structure and be with relatively long lifetime of the UCL states. At least two energy gaps among states should match with the sensitizer excited state relaxation. As shown in Fig. 2.1, Pr^{3+}, Nd^{3+}, Sm^{3+}, Eu^{3+}, Tb^{3+}, Dy^{3+}, Ho^{3+}, Er^{3+} and Tm^{3+} are luminescent and can be explored as activators.

With the effort of a lot of researchers, upconversion nanochemistry has been well developed, regarding control of nanoparticle size from the scale of nanometers (*e.g.*, 3 nm[26]) to several hundreds of nanometers (*e.g.*, 400 nm[27]), phase (*e.g.*, α-$NaYF_4$ to β-$NaYF_4$[28]), morphology (*e.g.*, spherical to cylindrical[14]), hierarchical structure (*e.g.*, core to core-multiple shell[29]), doping concentration (*e.g.*, concentration of sensitizer/activator[30]), *etc*, targeting for specific applications. In order to make the UCNP related applications practical, high UCL intensity is required. Therefore, various strategies have been investigated to enhance UCL intensity.

Size and morphology manipulation can be used to enhance the UCL intensity to some extent. Usually, large size and structure with low surface area-to-volume is beneficial for bright UCL due to suppression of surface quenching. Doping concentration modification itself can enhance UCL but which is subject to the rise of concentration quenching. The most well developed and efficient strategy to

produce high quality of UCNPs is through core-shell/core-multi-shell hierarchical architecture manipulation. Core-shell structures have many benefits, such as spatially separating dopant ions, reducing surface-related quenching, enhancing light harvesting, separating ions from core to shell to suppress deleterious cross relaxation (CR) and tuning upconversion colors, *etc.*[31] Depending on the function of the design, different hierarchical architectures are applied.

To suppress surface quenching, usually an inert most outside layer with no dopants is grown epitaxially, *e.g.*, $NaYF_4$:Yb^{3+}/Ln^{3+}@$NaYF_4$ (Ln = Er or Tm).[32–36] The shell layer shields the core from the environment and the surface ligands to reduce surface quenching, as illustrated in Fig. 2.2a. For example, the quantum yield (QY) of $NaYF_4$:Yb^{3+}/Er^{3+}@$NaYF_4$ with one inert shell layer of $NaYF_4$ is 3 times higher than of the core $NaYF_4$:Yb^{3+}/Er^{3+} with the same size.[37] To enhance absorption, a core-shell structure can be applied for tuning monosensitizer or multisensitizer doping, to overcome low extinction coefficient and narrow band absorption of lanthanides to some extent, as illustrated in Fig. 2.2b.[38–41] For example, with the doping sensitizer Yb^{3+} present in both core and shell layers, $NaYF_4$:Yb^{3+}/Tm^{3+}/$NaYbF_4$/$NaYF_4$ core-active shell-insert shell gets a significant 11 times higher UCL enhancement compared to their $NaYF_4$:Yb^{3+}/Tm^{3+}/$NaYF_4$ core-insert shell counterpart.[42] In order to suppress deleterious CR to enhance UCL intensity, an inert transition layer could help to separate the emitters, as illustrated in Fig. 2.2c. For example, when a quenching-shield sandwich-structured $NaYF_4$:Yb^{3+},Ln^{3+}@$NaYF_4$:Yb^{3+}@$NaNdF_4$:Yb^{3+} (Ln = Er,Ho,Tm) is applied to separate emitter Ln from sensitizer Nd to avoid CR, the UCL is enhanced significantly compared to without the transition layer sample $NaYF_4$:Yb^{3+},Ln^{3+}@ $NaNdF_4$:Yb^{3+} (Ln = Er,Ho,Tm).[43] An extra benefit of this strategy is that it can be applied to multiple color imaging like orthogonal emission.[44–48]

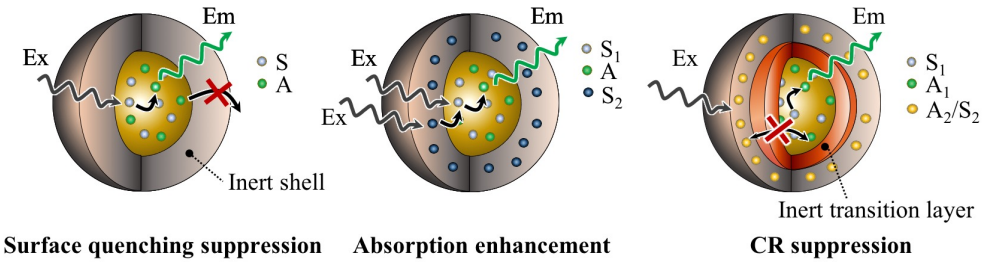

Figure 2.2: *Illustration of strategies for hierarchical architecture manipulation of UCNPs to enhance UCL intensity.*

2.3 Upcoversion mechanisims

2.3.1 GSA, ESA, ETU and CR

There are six fundamental upconversion mechanisms, *i.e.*, ground state & excited state absorption (GSA/ESA), energy transfer upconversion (ETU), cooperative upconversion (CU), cooperative luminescence (CL), cross relaxation (CR) and photon avalanche (PA). Among them, GSA/ESA, ETU and CR play significant roles in fluoride host material upconversion systems.[49] The contributions of CL and CU are in general 3-5 order less significant compared to ETU.[50] For PA to happen, rather strict conditions are needed to be fulfilled, like above threshold excitation power and sufficiently high activator doping concentration.

The upconversion mechanisms of GSA&ESA, ETU, CR and PA are shown in a simplified three energy level diagram in Fig. 2.3.[49] GSA is the process where he ground state of ions interact with incident photons and electrons and is excited to an excited state with relatively long lifetime. Then electrons at the excited state interact with the incident photons again and can be excited to a higher excited state, that is called ESA. The ions are excited through this ladder climbing process gradually to the UCL state. Consequently, the electron at the UCL state relaxes back radiatively to the ground state and an upconverted photon is emitted. In order to achieve high GSA&ESA upconversion efficiency, the energy structure of the activator should be of ladder-like configuration. Only a few lanthanide ions (Er^{3+}, Ho^{3+}, Tm^{3+} and Nd^{3+}) have this ladder-like configuration as shown in Fig. 2.1. Er^{3+}, Ho^{3+}, Tm^{3+} and Nd^{3+} are able to perform upconversion through this GSA&ESA mechanism. This GSA&ESA upconversion process only involves a single type of dopant, therefore, only one activator is enough and it is independent on the ion-ion distance. However, due to the small absorption cross-section of these elements, the upconversion efficiency is relatively low.

Energy transfer upconversion (ETU) is a more efficient upconversion method. In ETU systems, typically more than one type of rare-earth elements, *e.g*, a sensitizer with high absorption cross-section and an activator with multiple UCL emitting states, are doped. Energy transfer from the sensitizer excited state to the activator is identified as ETU, as shown in Fig. 2.3. The sensitizer is firstly excited through interaction with pump photons and excited to a metastable state. Then electrons at the metastable state of the sensitizer relaxes back to the ground state, transferring the harvested energy to the neighbour activator. An activator receiving several energy transfers in a row can be excited to a UCL emitting state in a ladder climbing way and then radiatively decay. The ETU process is sensitive

to the distance between the activator and sensitizer, which is determined by the dopant concentration. The correlation can be described in the formula below:[51,52]

$$P = \frac{1}{\tau_s}(\frac{R_0}{R})^s, \tag{2.1}$$

where τ_s is the effective lifetime of the sensitizer excited state including all the depopulation pathways except the energy transfer from sensitizer to activator. R is the distance between the sensitizer and the energy receiver ion. R_0 is the critical distance between the ions where the energy transfer rate equals the spontaneous decay rate of the sensitizer, and s is the index of multipolar reaction, with $s = 6$ representing dipole-dipole, $s = 8$ representing dipole-quadrupole and $s = 10$ representing quadrupole-quadrupole interaction. In anti-Stokes excitation methods, ETU is the crucial process playing a dominating role to excite activator ions. The common sensitizer-activator combinations with high brightness are Yb^{3+}-Ln^{3+} (Ln = Er, Ho, Tm) with excitation wavelength of ∼980 nm, and Nd^{3+}-Yb^{3+}-Ln^{3+} (Ln = Er, Ho, Tm) with excitation of both ∼980 nm and ∼808 nm.

The CR process, resulting from ion-ion interaction, could occur between the same type of activator ions, different type of activators, same type of sensitizers, and between activators and sensitizers. Its efficiency is dependent on the ion-ion distance and is therefore doping concentration dependent. The CR process affects the kinetics of UCL in many different ways. It is the main mechanism of concentration passive quenching of the UCL to reduce the intensity. CR can also lead to positive quenching which can play a significant role, *e.g.*, to the functioning of Tm^{3+}-doped silica fibre lasers.[53] CR is also the fundamental process for PA, see below.

PA is another upconversion mechanism which could happen in some circumstances, like high doping concentration and high power density excitation. The process involves ESA and CR, as illustrated in Fig. 2.3d. All ions are initially staying at the ground state, with no GSA resonance with the pump photons. Then with electrons of one ion pumped into the excited state, by whatever force (mechanical or optical), ESA resonates with the excitation pump photons matching in energy. Subsequently, the CR energy transfer between this ion and its neighbour ion promotes a self storage of both ions in a metastable level, leading to a looped metastable density increase pattern and stronger ESA intensity to the UCL state. Finally, the UCL state is populated to a significant level to observe the UCL phenomenon.

Except the above mentioned upconversion mechanisms, other undesired processes may happen during the UC as well, *e.g.*; nonradiative decay through multi-phonon relaxation, energy transfer to other impurity ions, ground state depletion.[50] In

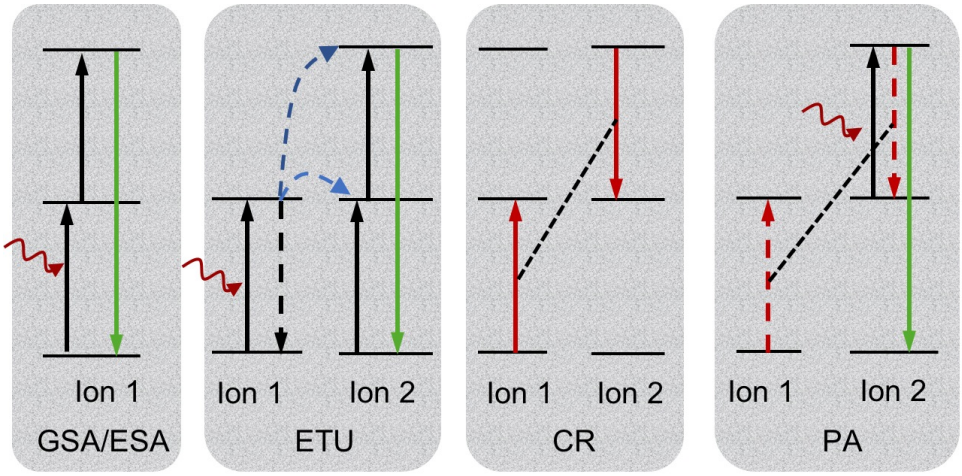

Figure 2.3: *Energy schemes for upconversion mechanisms of GSA/ESA, ETU, CR and PA.*

order to achieve high brightness of the UCL, these processes should be suppressed to the level that they do not dominate over the upconversion process.

Due to the nature of these upconversion mechanisms, UCL of UCNPs exhibits excitation-dependent optical properties, *e.g.*, excitation wavelength dependence, power density dependence, excitation pulse duration response and excitation pulse frequency response, which will be discussed in detail in the next sections.

2.3.2 Excitation wavelength response

With doping more than one type of UCNPs sensitizer, the UCNPs can be excited by more than one wavelength excitation through either anti-Stokes excitation or Stoke excitation. For both methods, the energy gap between the ground state and the targeted excited state should match with the incident photons energy, with small deviation allowed to be compensated by multi-phonon assist. A relatively high absorption cross-section of the sensitizer is necessary in order to produce measurable PL intensity. These regulations put restriction on the choice of wavelength excitation. For pumped upconversion of the GSA/ESA mechanism, due to the ladder-like energy level structure, the incident photon energy should match with at least two energy gaps among the ladder-like energy states and be resonant with both GSA and ESA transitions. For GSA/ETU, the incident photon energy should match with the sensitizer energy gap between the excited state and ground state, *i.e.*, be resonant with the GSA transition of the sensitizer. In order to produce measurable UCL intensity through the ETU process, the resonance between

the sensitizer relaxation and activator excitation (both GSA and ESA) should be strong. For the reasons above, a 980 nm laser diode is a good anti-Stokes excitation candidate since 980 nm photons resonance well with the ground state excitation of Yb^{3+} in the Yb^{3+}-sensitized GAS/ETU upconverting system. 808 nm is another commonly applied anti-Stokes excitation wavelength for strong resonance with the ground state excitation of Nd^{3+} in Nd^{3+}-sensitized GSA/ETU upconverting systems or with Er^{3+} GSA/ESA for solely doped GSA/ESA upconverting systems. Under high dopant concentration, another upconversion mechanism, namely PA, could happen if the power is above the threshold. In this scenario, the excitation photons only need to be resonant with the excited state absorption of the dopants without GSA, then leading to self storage of the metastable level through the CR process, as illustrated in Fig. 2.3d. For example, 750 nm and 840 nm wavelengths can be applied as being resonant with the excited state of Ho^{3+} doped fluorozirconate glass.[54]

Depending on the excitation wavelength, the kinetics of the UCNPs varies. Through the anti-Stokes GSA/ETU excitation method, the kinetics of the UCL state is a comprehensive temporal response of the whole UC system to the function of excitation, decided by the effective lifetime of the sensitizer, including all the pathways, lifetime of intermediate states and UCL emitting state of the activator. Usually, the energy migration between sensitizer and activator is the dominant factor affecting the kinetics of the UCL emitting state considering that it is usually the slowest step among the upconversion related processes. Through the Stokes GSA/ESA excitation method, the UCL emitting state is independent on the intermediate state and is free from the effect of the sensitizer when the energy back transfer from activator to sensitizer is nonsignificant. Therefore, the Stokes method is considered to be more applicable than the anti-Stokes method to obtain the intrinsic lifetime of the UCL emitting state (Paper II).

2.3.3 Power density response

Due to the nature of the sequential absorption of two or more excitation photons of UCL, the UCL emitting intensity exhibits a nonlinear power density dependence. The power dependence of the PL at static states has been studied systematically by Pollnau *et al*, and many other groups, through a simplified rate equation model formulating the population density of each state corresponding to time.[55,56] If the underlying upconversion mechanism is GSA/ESA or ETU, the mechanism can be determined by the power intensity - UCL intensity correlation to some extent under low power. However, in a real UCL measurement, the upconverting mechanism is more complicated; the saturation effect and additional processes, *e.g*,

CR between excited ions and ground state depletion under high power intensity, may play nonnegligible roles. As a result, other efforts are needed to determine the mechanism.[56,57]

Due to the nonlinearity of the UCL, the QY of UCNPs is power density dependent and increases with power density. Note that due to the power density dependence characteristics of UCNPs, a high photon conversion capacity is guaranteed by a high excitation power.[58] Therefore, a way to spatially modulate the excitation light to enhance the excitation intensity would be a good strategy to enhance the upconversion QY, which will be discussed in detail in chapter 4.

2.3.4 Excitation pulse duration response (same frequency)

The UCL time correlated intensity profile in terms of the impulse response function (IRF) is often characterized under pulsed excitation, and should ideally be a $\delta(t)$ excitation function with infinitely small pulse width. However, in practical experiments, the pulse width of the excitation function is not infinitely small with an excitation profile to be square wave shaped with short duration of time. As a result, the optical response to the excitation is the convolution of the IRF and a pulsed excitation function, determining the dependence on the kinetics of the pulse duration of the upconversion system. Depending on the upconversion mechanism of the system, the pulse duration dependence will be different.

Different states are populated to different degrees under the duration of pulsed excitation. For the GSA/ESA upconversion mechanism, under a pulsed excitation, the UCL happens immediately at the onset of excitation, exhibiting a very fast rise and a monoexponential decay profile with the decay time constant decided solely by the intrinsic lifetime of the UCL emitter. Within the duration of the pulsed excitation, the UCL emitting state is constantly populated from the onset of the pulse until the end of the pulse and the intensity starts to decrease right away after the end of the pulse. For the GSA/ETU mechanism, the UCL emitting state is not directly pumped by the incident photons, instead it is pumped by the energy transfer between sensitizer and activator. Due to the fact that the building up time of the UCL through energy migration from sensitizer to activator is relatively long following a pulsed excitation, a profile with a relatively slow rise and decay behaviour will be observed. After the pulsed excitation, the UCL emitting state is still pumped, due to the long intermediate lifetime, and then the UCL intensity starts to decrease.

When applying a periodic modulated excitation source with varied pulse duration but with same frequency, PL spectra with varied intensity ratio of different UCL

bands will be observed under whatever upconversion mechanism. This would lead to an overall varied UCL color output. It is of significant importance to study the pulse duration response for extended applications due to the above mentioned pulse duration response property. For example, different color outputs resulting from varied excitation pulse widths are applied as one optical encoding dimension. Taking advantage of the nonlinearity of the UCNPs, some strategy has been proposed to temporally modulate the excitation photon distribution to boost the UCL.[59,60] Under the same average power density and with application of quasi-CW excitation (*i.e.*, pulsed excitation with duration of μs to ms range) can enhance the UCL by orders of magnitude compared to equivalent CW excitation. Also the UCL pulse duration response can be used as an optical encoding dimension for extended UCNP applications (paper IV). What is more, the common way of fitting the time correlated intensity profile into biexponential components to extract the constants of decay time τ_d and rise time τ_r can be invalid under long durations of the pulsed excitation. This must be understood for the sake of optical characterization.

2.3.5 Excitation pulse frequency response

Due to the different building up time periods of UCL states, different UCL emitting intensities can be observed under pulsed excitation with different frequencies, but with same duty cycle and average power (and same total pulse duration under specific time range). Generally, with increasing pulsed excitation frequency, the pulse duration is too short for the UCL related states to be populated to a significant level, and the UCL emitting intensity would then show a decreasing trend. This pulse frequency dependence property of UCL has been investigated to identify NIR excitation wavelengths (between 808 nm, 980 nm and 1540 nm) with an UCNP equipped NIR photodetector (paper V).

2.4 Synthesis of upconversion nanoparticles

Methods to synthesize UCNPs mainly include the coprecipitation method,[61] the thermal decomposition method,[33] and the hydrothermal/solvothermal method.[62,63] The effect of reaction conditions (reaction time, temperature and raw materials), also together with doping concentration, doping ion type, *etc*, have been well investigated by many researchers.[62,64]

The solvothermal method to synthesize UCNPs is one of the most popular methods due to low cost, time efficiency and high quality products.[63,65,66] Both coordinate and noncoordinate solvents are used. Solvents with high boiling point

like 1-octadecene (ODE) (315°C) is often used as the noncoordinating solvent to provide a high temperature reacting environment. Coordinate solvents like oleic acid (OA) with excellent coordinating ability can be applied to surface modify the UCNPs to increase solubility in organic storing solvents like cyclohexane/hexane and also to avoid UCNP aggregation. In a typical solvothermal method of core UCNPs, a lanthanide source powder with specific molar proportions is dissolved in a solution of ODE and OA under heating (*e.g.*, 150°C) in argon atmosphere to form a homogeneous solution in a three-neck flask (typically with volume of 100 ml/250 ml). After the precursor solution is cooled down to room temperature, a methanol solution of NaOH and NH_4F with specific molar ratio is added and the mixture is stirred and heated (to *e.g.*, 80°C) and maintained to evaporate methanol. Subsequently, the solution is degassed, quickly heated to a high reacting temperature(*e.g.*, 300°C), and kept for hours, depending on the size requirement, under the protection of an argon atmosphere. The mixture is then cooled down and the nanoparticles are purified through centrifugation using ethanol and water. The supernatant is discarded, and the precipitate is finally suspended in cyclohexane/hexane and stored. The procedure to epitaxially grown shells on the core UCNP structures is similar to the core synthesis. This solvothermal method makes it possible to synthesize high quality of α/β-phase UCNPs. The size can be tuned within the scale of several nanometers to hundreds of micrometers with narrow size distributions.

Although the solvothermal decomposition can produce monodisperse, single crystallized, well-defined and pure phase nanoparticles, there are still some shortcomings of this method, like high temperature reaction conditions (above 300°C) and relatively complicated experimental protocols. Therefore, an even simpler experimental protocol with relatively mild reaction conditions has been developed; the one-step hydrothermal method. In this method, UCNPs grow within a sealed environment under high pressure and high temperature (usually above a critical point of the solvent). A reactor like autoclave is usually used in the experiments to provide a sealed condition. Organic solvents like OA, EDTA is used as capping ligands to control the size and morphology of the UCNPs and to prevent UCNPs aggregation. The main reacting system is often ethanol-water-OA based.

In a typical hydrothermal synthesis method of core UCNPs, raw materials like NaOH, ethanol and OA are mixed together to form a uniform transparent solution. Stoichiometric stock water solutions of RE complexes containing Ln sources with specific molar proportions for the host material and doping ions are added into the mixture mentioned above. Finally, an aqueous NH_4F ethanol solution is subsequently added into the mixture and stirred under 45°C to form a milky solution. Subsequently, the milky solution is transferred into a 50-mL Teflon-lined

autoclave and heated to some temperature (*e.g.*, 200°C) and is there remained for a couple of hours under protection of inert gas Ar_2, depending on size and morphology requirement. After the reaction, the products are cooled down in air in room temperature. Subsequently, the products are precipitated through centrifugation. The obtained nanorods are then washed several times and are finally dispersed in cyclohexane/hexane for subsequent use. The synthesized core UCNPs can be applied to synthesize core-shell structured UCNPs through the solvothermal method described above.

UCNPs synthezied by both methods have limited water solubility due to the surface capping of organic hydrophobic ligands (for example OA), therefore, a surface modifications of the UCNPs is required in order to improve the UCNP water solubility, like inorganic inert shell growth,[67] surface ligand washing (wash OA with HCl acid),[68] surface treatment with inorganic ligand layers (exchange OA with $NOBF_4$),[68] or surface modification with other water soluble organic capping ligands (*e.g.*, oleyl amine (OM))[69] for specific practical applications.

2.5 Characterization of upconversion nanoparticles

There are mainly two types of characterization of UCNPs: morphological and optical. Morphological characterization is to study the information regarding size distribution, crystal structure, composition distribution and other physical properties of the UCNPs. Optical characterization involves absorption/transmittance, lifetime determination, photoluminescence spectra and UCL determination.

2.5.1 Morphology and structure characterization

The structural and morphological characterization can be performed by transmission electron microscopes (TEM), X-ray diffraction and Scanning Electron Microscopy (SEM). Energy-dispersive X-ray spectroscopy (EDX) can be used to study the distribution of elements of the UCNPs.

2.5.2 Optical characterization

The optical characterization is usually performed in solvent conditions, like cyclohexane/hexane in a cuvette made from glass, sapphire, fused quartz or plastic. A beam of excitation photons is passed through the cuvette, being scattered or absorbed, to measure the absorption/transmittance, photoluminescent intensity, and lifetime of the photoluminescence.

Absorption characterization

The room temperature absorption of UCNPs is usually performed with a xenon lamp with wavelengths that cover the UV-Vis-NIR range and with the radiation passing through the sample and detected. An absorption spectrum will have its maximum intensity where the absorption is strongest. When a light beam with intensity i_0 passes through the sample, the transmitted intensity is described as:

$$I_t = I_0 e^{-\alpha L} \approx I_0(1 - \alpha L) \tag{2.2}$$

under low absorption conditions. Here $\alpha = \sigma N_i$ is the absorption coefficient, which is dependent on the absorption cross-section σ of the corresponding absorption transition and the population density of the absorbing state N_i. L is the light passing length. Therefore, after light passing the sample depth of L, the absorption is:

$$I_0 - I_t \approx I_0 \alpha L = \sigma N_i L I_0 \tag{2.3}$$

Due to the relative insensitivity of the crystal field of $4f$ orbitals, UCNPs have narrow absorption spectral profiles.

Photoluminescence characterization

Photoluminescence characterization is performed by detecting the luminescent intensity to obtain the spectroscopy after an excitation. Both anti-Stokes excitation and Stokes excitation static photoluminescence measurements can be performed with commercially available and widely used spectrophotometer setups. For anti-Stokes excitation, laser diodes with wavelengths in the NIR, like 808 nm and 980 nm, are utilized to excite the sample. By the Stokes excitation method, laser diode of wavelengths in the visible range is applied (*e.g.*, 485 nm laser diode) for excitation.

Luminescence kinetics characterization

Time-resolved luminescence measurements are recorded after a periodic pulsed excitation (usually with wavelength in the NIR range, *e.g.*, 980 nm and 808 nm) from a laser diode often through the anti-Stokes excitation method. With the excitation laser passing through the samples, the emitted photons from the UCNPs are detected by a time-correlated single-photon counting component (TCSPC). Through fitting the curve with a simplified biexponential formula, the constants τ_d and τ_r can be extracted and usually interpreted as the rise time and decay

time of the PL, respectively. Both rise time and decay time (lifetime) are mean values, which represent the average time of population of the UCL state assembly to increase from $1/e$ of its maximum value to its maximum value or *vice versa*. It should be noted that, instead of interpreting τ_d as an intrinsic lifetime, the constant should be interpreted as the comprehensive temporal response of the UC system to the function of excitation since other intermediate states are involved in the UCL process. This will be further discussed in detail in chapter 3. Another way to obtain the intrinsic lifetime is to excite the activator directly from the ground state to the UCL emitting state through the Stokes excitation method without involving intermediate states of activator and sensitizer. This method is more precise when the dopant concentration of sensitizer and activator is low. Under high dopant concentration, extra decay channels of the UCL emitting state through the CR process starts to play a nontrivial role in the system and accelerate the decay speed, leading to a smaller decay constant than the intrinsic lifetime.

UCL characterization

Nowadays it is still often difficult to compare different UCL results in a meaningful way, partly due to the power intensity dependence of UCL and the results reported are usually under one single power density excitation condition, which complicates the comparison between different research works. Therefore, the QY has often been chosen as the descriptor to indicate the UCL properties and provide a way to compare among reported group works. QY is defined as the ratio of the number of emitted photons to absorbed photons. There are direct and indirect ways to measure or estimate the QY of an upconversion system. The straightforward one, most common and accurate way of quantifying the QY directly is through using an integrating sphere.[70,71] The mechanism of integrating sphere measurements involves emitted light from samples reflecting on the inner surface multiple times and finally being detected at the exit ports. The absorbance of the sample is measured as reference. Therefore, the QY, is calculated based on a reference sample with already known QY. Through the spectrofluometer-based method, a reference sample with known QY is also needed and the UCL and absorption are measured by the spectrometer. With both methods, the absorbance of the sample should be measurable (> 0.03) in order to get the value of the QY at the excitation wavelength and a reference sample is needed which limits the testing conditions. Also the QY can be measured under only a single power density condition. Since the QY is power dependent, it is of interest to quantify the power dependent QY under more power conditions through indirect ways. For example, the power dependent QY can be estimated based on rate equation models with parameters

appropriately chosen, which will be discussed further in chapter 5.[70,72,73] So far, a relatively high upconversion QY of 7.8 % at the power of 22 W/cm^2 for a $NaYF_4$: Yb^{3+}, Er^{3+} has been reported.[70]

2.6 Emerging applications of UCNPs

The required low excitation power density, the ability of efficient frequency upconversion at NIR, the easily defined upconversion wavelength, as well as the nanometer size dimension are facts that promise the use of light upconversion materials in information technology, bioimaging as well as for solar cells. These endeavors originate from a few main stimuli: (1) The use of light excitation lying in the NIR range that is invisible to naked eyes and bio-transparent and with emission lying in visible range, is ideal for anti-conterferting and bioimaging purpose; (2) Tunable emission colors at a number of wavelengths with narrow profile, without overlap, by excitation at one single wavelength with multiple display ability makes it promising for information storage; Furthermore, (3) frequency up-conversion of IR can be useful for harvesting IR photons for their conversion to higher energy photons which can then readily be absorbed by current solar cell materials. Although encouraging results have been recently obtained, there remain hurdles to their practical use, including: (i) Weak and narrow IR absorption due to the nature of f-f transitions: (ii) Limited assortment of wavelengths for upconversion excitation and its utilization for solar energy conversion of IR photons: (iii) Relatively low upconversion efficiency. The development in each application and strategies to overcome obstacles for practical applications will be discussed below to obatin a deeper view of the UCNPs-related applications.

2.6.1 Bioimaging application of UCNPs

Due to the requirement of life-quality improvement, life science and medicine are developed very fast, which has stimulated investigations in the area of bioimaging. Bioimaging is a noninvasive method to visualize biological processes, leading to observation of subcellular structures, entire cells, tissues and up to entire multicell organisms. It provides morphological, physiological and other information of biosamples and organisms. UCNPs have the ability to be excited by biologically transparent NIR light (*e.g.*, 800 nm, 980 nm) and emit multi-wavelength light within shorter-wavelength in NIR, Vis and even UV range. Due to the optical properties of UCNPs, such as photoluminescence of high chemical and physical stability, low cytotoxicity, low cost to synthesize, low auto-fluorescence, deep tissue penetration, good photostability, big anti-Stokes shifts, non-photobleaching

and sharp emission, UCNPs have become unique candidates for medical bioimaging, including *in vivo* or *in vitro* imaging of animal tissues.[74]

UCNPs for constructing high contrast imaging have been investigated for many bioapplications so far: cellular imaging, whole animal deep depth PL imaging, optical tomography, multimodal imaging.[75] Zhang *et al.* first reported application of folic acid-conjugated $NaYF_4$:Yb^{3+}/Er^{3+} UCNPs for cellular imaging on human HT29 adenocarcinoma cells and human OVCAR3 ovarian carcinoma cells.[61] Then later one, Nyk *et al.* reported high contrast imaging of human pancreatic cancer cells using $NaYF_4$:Yb^{3+}, Tm^{3+} UCNPs with a complete absence of autofluorescence through NIR excitation-NIR emission.[76] The NIR-NIR upconversion allows high contrast in vivo bioimaging and deep tissue penetration, therefore using both NIR excitation and NIR emission is desired for *in vivo* imaging of small animals and utilized by many research groups,[15,77–79] as both absorption and scattering of excitation and emission are reduced. After Nyk *et al.*, deep tissue bioimaging UCNPs are improved to be more efficient with high luminescent brightness and the imaging depth is able to reach 3.2 cm.[80]

Due to the nonlinearity of UCL, the UCL intensity decreases exponentially with tissue depth, leading to weak bioimaging signals at deep tissue positions. Therefore, it is of fundamental significance to enhance the UCL intensity of the UCNPs to further increase bioimaging depth. The main strategies to tune PL intensity for effective bioimaging include: 1) PL intensity tuning through chemical modification. The chemical modification can include dopant concentration modification, core-shell/size architecture modification, UCNP surface modification, host material and host matrix modification; 2) PL intensity tuning through optical modification. Optical modification can include plasmonic effect enhancements,[81] excitation function modification,[58] excitation light propagation modification (paper I and IV).

Common dimensions explored for bioimaging purpose with UCNPs include static /dynamic UCL color output, lifetime of UCL bands of interest. In order to extend bioimaging color channels, static multicolor output tuning under CW stimuli through orthogonal emission with multiple emitters doping (spatially separated through taking advantage of core-inert layer-shell structure),[48] dopant concentration modification,[30] power intensity modification,[30] transition metal doping[82] and other strategies are applied. Moreover, dynamic color emission under pulsed excitation can be achieved by manipulating non-steady state of energy transfer upconversion and tuned to increase channels. By changing excitation from CW to pulsed excitation, due to different building and decay time of each UCL emitting band, the dynamic color output can be tuned by adjusting the pulse duration and

pulse frequency of excitation. Moreover, the lifetime of UCL emitting bands can be of interest as a bioimaging dimension as the UCL is intensity independent. It overcomes the restriction of intensity dependence of the UCL and large lifetime difference of the samples are therefore preferred for better distinguishing.

2.6.2 Optical encoding applications of UCNPs

Optical information technology is the technology to store, manipulate, communicate, transfer information (biological, physical or chemical) through optical processes, *e.g.*, data storage, document security encoding, anti-counterfeiting, barcoding and remote-control photoswitching. Optical encoding plays significant roles in these applications. The optical characteristics of fluorophore materials utilized for optical encoding determines the decoding and encoding efficiency. Among several optical encoding fluorophores, organic dyes, which are commonly used for optical encoding, are not considered as ideal. The spectrum overlap between excitation and emission can strongly interfere the interpretation of the signal. The poor photostability and wide emission band also constraint the applications of organic dyes for optical encoding. QDs form a popular alternative for organic dyes as they have narrow and tunable emission bands with photostability and chemicalstability. However, the toxicity of QDs is a big drawback for their bioapplications. UCNPs are promising candidates for optical encoding that surpass organic dyes and QDs. The large anti-Stoke shifted emission bands guarantee a distinct emission spectrum from the excitation spectrum; as discussed above it can show multiple sharp emission bands with multiple colors as combinatorial codes. UCNPs are resistent to photodestruction and show low background autofluorescence. UCNPs futhermore possess tunable morphology with size ranging from a few nanometers to hundreds of nanometers and the application of core-shell hierarchy architectures can be used to reduce quenching and biotoxicity.

Many optical encoding dimensions of UCNPs have been applied as encoding elements, *e.g.*, UCL emitting band spectra,[10,16,83,84] ratiometric intensity of emission bands,[85,86] luminescence lifetime,[87,88] phase shift of emission to excitation[89] and temporal response (paper IV). The wavelength of an UCL emitting band is the most commonly used parameter as optical encoding channel as it is straight forward to decode, easy to perform experimentally and is flexibly tunable through modification of size or core-shell structure. To induce color emission bands, multi-activator ion doping is a common strategy,[85] *e.g.*, Qin *et al.* reported doping of Tb^{3+}, Eu^{3+}, Dy^{3+} and Sm^{3+} to produce colors of purple, red, green, orange and blue.[84] The method of ratiometric intensity of emission bands can easily be used without the request to invent new emission bands, *i.e.*, the UCL intensity

ratio between emission bands can be manipulated through regulating UCL dynamics as encoding channels. For example, Gorris *et al.* investigated the dual emission encoding through adjusting the intensity ratio of the code emission band and reference emission band.[86] It is to be noted that the wavelength and the ratiometric nature of the emission bands as coding dimensions have their limits as there are limited available colors and because the fluorescence intensity ratio is difficult to be manipulated precisely due to factors of light scattering, absorption, high signal-to-noise requirements. Therefore, lifetime as decoding dimension has been investigated quite much as it is independent of luminescence intensity and can be tuned in a large range from nanoseconds to milliseconds,[87] which provide a much bigger data encoding capacity. In the meantime, specialized equipment like fluorescence lifetime imaging microscopy (FLIM) and cameras capable of a short exposure time of nanoseconds are required. To combine wavelength and the ratiometric nature of emission bands, lifetime methods provide a good strategy to further increase information storage capacity.[87,90] The phase angle of emission relative to excitation can be applied as encoding dimension, which can also be combined with color as dual optical encoding.[89] The idea of temporal response as optical encoding dimension is to apply a periodic modulated excitation source with a period bigger than the relaxation time of the encoding luminescent state, the state is populated to different degrees depending on the repetition and duration of the pulses. Therefore, the overall color output will vary and the kinetic constants of the UCL, extracted from the curve of time-averaged state population *vs* pulse duration, can be applied as an optical encoding dimension, reflecting the corresponding population variation of the luminescent states induced by changes in the pulse characteristics.

2.6.3 UCNP sensitization of photovoltaic devices

Photovoltaic devices are attractive electrical devices which are capable to transfer solar energy directly into electricity, which is environmental friendly using an energy resource that is unlimited. It has drawn huge amount of attention worldwide, especially when the discussion of global warming is at heat. We have all heard the teen climate activist Greta Thunberg saying "How dare you?" to evoke the society's awareness to reduce the extensive use of traditional fossil energy. The development and utilization of clean, green and renewable energy is necessary and urgent. Solar energy is believed to be potentially the future of our earth as it is the cheapest, cleanest energy resource and easier to get access to, compared with its counterparts wind energy, hydroelectric, tidal energy geothermal and other types. In order to make our earth's future brighter, the efficiency of solar cells needs to be improved

more in order to be commercialized. The infrared region (IR), containing almost half of the solar irradiation, is not well utilized by contemporary photovoltaic devices due to the limited absorption of IR of the solar cell materials.[91,92] UCNPs have been considered to be a potential candidate to increase photovoltaic devices efficiency due to their ability to upconvert NIR light into shorter-wavelength IR, Vis, or even UV range,[13,93–97] which can then be absorbed by photovoltaic devices. This can provide a strategy to collect the energy loss from IR range for photovoltaic devices and further improve their efficiency, which would broaden the absorption range. What's more, UCNPs can be easily produced and packaged into solar cells. For example, Yuan *et al.* produced UCNPs embedded solar cells and obtained an enhancement of the solar cells efficiency.[98,99] There are though some obstacles for UCNPs sensitizing solar cells, *i.e.*, the QY of UCNPs is low under solar irradiance, the absorption cross-section of UNCPs is small, the absorption spectra range of each doped Ln is narrow, as a result, the contribution from UCNPs under solar irradiation could be too low to make a significant difference to solar cells efficiency. Therefore, some strategies have been applied to overcome these obstacles. Chen *et al.* applied dye-coated UCNPs to dramatically enhance the absorption of UCNPs, then to further sensitize DSSCs.[100] Compared with a control sample without dye-coated UCNPs, there was an overall solar cells efficiency enhancement of 13.1%. Another well explored way to enhance the NIR absorption of UCNPs sensitized photovoltaic devices is through the plasmonic effect.[101] Due to the surface plasmon resonance, the local electric-magnetic field around the metallic particles is dramatically enhanced. When UCNPs are put in this strong electromagnetic field, the absorption cross-section of the UCNPs are enhanced. A 8.4% (relative) efficiency enhancement of perovskite solar cells with UCNP-incorperated plasmonic substract is reported by Park *et al.*[81] Except increasing the absorption, another strategy is to broaden the absorption range. Instead of doping solely one type of sensitizer, multi sensitizer doping, (*e.g.*, using both Yb^{3+} and Nd^{3+}), can be applied to broaden the absorption range. For increasing the QY of UCNPs, a light spatial modifier has been applied and an overall solar cell enhancement of 9.51%, compared to a control sample without any UCNPs sensitization, has been reported (paper III).

2.6.4 UCNP-based narrow-band near-infrared photodetectors

The existing NIR photodetectors often focus on broad band detection.[102,103] Some of them are able to detect the visible range simultaneously as the NIR range.[104–108] Group III-V semiconductors, *e.g.*, InGaAs, based NIR photodetectors, have been extensively explored[109]. The challenge is to design narrow-band detection of NIR

photodetectors with low visible light noise and high sensitivity in the output signals for specific applications.[110] UCNPs have been explored for fabricating NIR photodetectors for narrow band detection.[111] Zhang *et al* have combined UCNPs together with MoS_2 to achieve 1000 times enhancement of both responsivity and detectivity at 980 nm excitation, compared to pure MoS_2.[112] Wu *et al.* have explored UCNP driven graphene/GaAs heterostructure and reached detectivity of $1.1 \times 10^{11} Jones$ for 980 nm detection.[113] To the best of knowledge, the highest till date reported responsivity is 2.7×10^4 AW^{-1} (for UCNPs/graphene),[111] and the detectivity is meaasured to $1.05 \times 10^{15} Jones$ for MoS_2-UCNP[114] for the UCNPs category of photodetectors (@980 nm, 1V). In paper IV, the combined NIR detector structure of microlens array/Au NRs/UCNPs/$MAPbI_3$ has reached both high responsivity and detectivity and fast response time of $\sim$100 ms.

Chapter 3

Upconversion luminescence kinetics upon short pulse excitation

3.1 Introduction

The decay kinetics of UCNPs is one of the fundamental aspects for dynamics related applications, like bioassay, optical encoding and bioimaging. Usually, the UCL decay is characterized by an anti-Stokes excitation method. The time correlated luminescence intensity profile of the UCL emitting band of interest is detected after a short pulsed excitation, usually in the NIR range. The rise and decay time constants τ_r and τ_d of the luminescence are usually extracted by fitting the time correlated luminescence intensity curve with the formula below:[73]

$$I(t) = I_0[e^{-\frac{t}{\tau_r}} - e^{-\frac{t}{\tau_d}}], \tag{3.1}$$

where I_0 is a scaling constant. Under this simplified two component decay profile model, all the emitting centers are considered to behave in the same way in a periodic crystallized field. Usually, the population and depopulation of each UCL state involves several states, therefore, the constants τ_r and τ_d are mean values representing the effects of all the processes. This simplified two component model is limited for expressing the individual pathways, therefore, numerical or analytical analysis of decay kinetics of the UCL state can be required to better study these pathways.

3.2 Standard two-photon upconversion model

Simulation models can provide powerful theoretical methods to understand the UCL kinetics of UCNPs. Time-dependent rate equation models have thus been

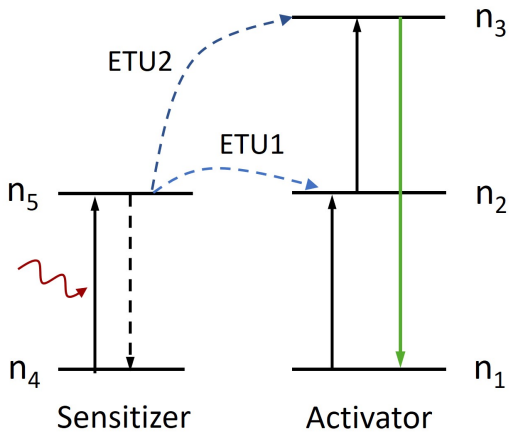

Figure 3.1: *Energy transfer upconversion (ETU) scheme for standard two-photon upconversion luminescence*

applied to theoretically study the kinetics of UCL. These models deal with time correlated population changes of each state with the assumption that same type of ions are in a homogeneous environment, leading to equal optical kinetics.[115] A set of coupled first order differential equations describing the population change with time is modelled. With such a model, the influence of the lifetime of the intermediate state, the CR process, energy transfer and power density dependence and other elements on the decay kinetics of UCNPs can be studied. Depending on the properties of the UCL emitting state, models with different complexity, *i.e.*, different number of relevant states included in the model system, can be applied.

Simplified two-photon upconversion models are reported in many works in order to provide a reasonable description of the UCL mechanism for co-doped systems, *e.g.*, green UCL emitting of Yb^{3+}/Er^{3+} co-doped system.[72,116,117] In a typical two-photon upconversion model, as illustrated in Fig. 3.1, there are in total five energy states; ground state and excited state of the sensitizer (a typical energy structure of Yb^{3+}), and ground state, first excited state and UCL emitting state of the activator. With ETU being the main upconversion mechanism, sensitizer absorption resonats with excitation photons and activators are excited through energy transfer from sensitizers sequentially to the UCL emitting state. When electrons at the UCL emitting state decay radiatively to the ground state, upconverted photons are emitted. In such a model, the energy decay from the highest state to intermediate excited states of the activator is neglected.

This model is representative when the UCL emission is a two-photon process with ETU as the upconversion mechanism, *e.g.*, the 525/540 nm UCL emitting band

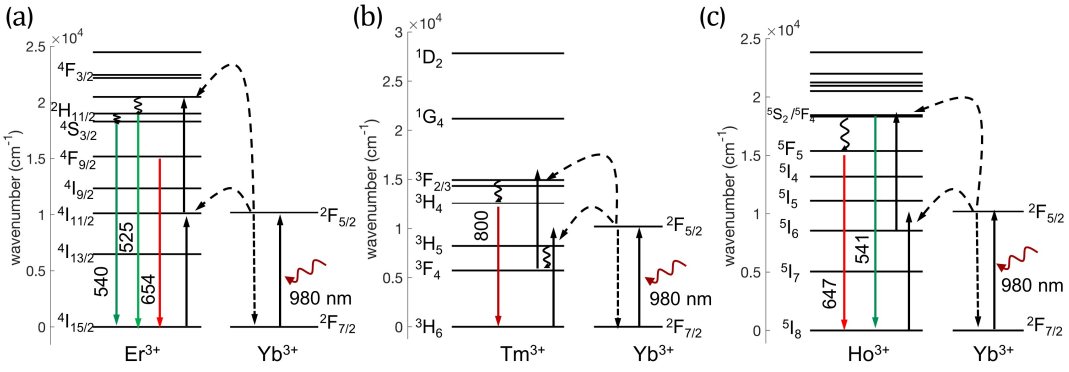

Figure 3.2: *a) Energy diagram of the green (525/540 nm) emitting of Yb^{3+}/Er^{3+} co-doped system, b) Energy diagram of the 808 nm emitting of Yb^{3+}/Tm^{3+} co-doped system, c) Energy diagram of the green (541 nm) emitting of Yb^{3+}/Ho^{3+} co-doped system.*

of Er^{3+}/Yb^{3+} co-doped system,[118] the 800 nm UCL emitting band of Tm^{3+}/Yb^{3+} co-doped system[119] and the 541 nm UCL emitting band of Ho^{3+}/Yb^{3+} co-doped system,[120] with UCL mechanisms depicted in Fig. 3.2. In Fig. 3.2a, green emission of Er^{3+} is pumped by two photons sequentially from Yb^{3+} (sensitizer) relaxation of $^4F_{5/2}$ to $^4F_{7/2}$ through two ETU processes with rate constants of W_1 and W_2, respectively. Then Er^{3+} ions non-radiatively relax to the UCL green emitting state $^2H_{11/2}/^4S_{3/2}$ from the $^4F_{7/2}$ state and thereafter radiatively decay to the ground state $^4I_{15/2}$ with one photon emitted. In the simplified three energy level with the activator described in Fig. 3.1, the energy level population of n_1, n_2 and n_3 can represent the population of $^4I_{15/2}$, $^4I_{11/2}$ and $^2H_{11/2}/^4S_{3/2}$ and n_4, n_5 can represent population of state $^4F_{7/2}$ and $^4F_{5/2}$ of Yb^{3+}. Similarly, in Fig. 3.2b, the NIR 800 nm UCL emitting band of Tm^{3+} is pumped by two ETU steps from the sensitizer Yb^{3+} and n_1, n_2, n_3, n_4 and n_5 can represent the population of $^3H_6$, $^3F_4$, $^3H_4$ of Tm^{3+} and $^2F_{7/2}$, $^2F_{5/2}$ of the sensitizer in this model. In Fig. 3.2c, n_1, n_2, n_3, n_4 and n_5 can represent the population of $^5I_8$, $^5I_6$, $^5S_2/^5F_4$ of Ho^{3+} and $^2F_{7/2}$, $^2F_{5/2}$ of sensitizer Yb^{3+}. Therefore, this model can represent several cases and be applied to study the mechanism of two-photon UCL.

Based on the model in Fig. 3.1, the time-dependent population of each energy state under excitation can be described by the equations below:

$$\text{State 1} : \frac{dn_1}{dt} = -W_1 n_5 n_1 + \frac{n_2}{\tau_2} + \frac{n_3}{\tau_3}, \tag{3.2}$$

$$\text{State 2} : \frac{dn_2}{dt} = W_1 n_5 n_1 - W_2 n_5 n_2 - \frac{n_2}{\tau_2}, \tag{3.3}$$

$$\text{State 3} : \frac{dn_3}{dt} = W_2 n_5 n_2 - \frac{n_3}{\tau_3}, \tag{3.4}$$

$$\text{State 4} : \frac{dn_4}{dt} = -\frac{\sigma\rho(t)}{h\nu} n_4 + \frac{n_5}{\tau_5} + W_1 n_5 n_1 + W_2 n_5 n_2, \tag{3.5}$$

$$\text{State 5} : \frac{dn_5}{dt} = \frac{\sigma\rho(t)}{h\nu} n_4 - \frac{n_5}{\tau_5} - W_1 n_5 n_1 - W_2 n_5 n_2, \tag{3.6}$$

$$n_1 + n_2 + n_3 = n_{\mathrm{A}}, \tag{3.7}$$

$$n_4 + n_5 = n_{\mathrm{S}}, \tag{3.8}$$

where $n_i (i = 1 - 5)$ denotes the population of each state, $n_{A(S)}$ represents the density of the doped activator(sensitizer), τ_i (i = 2, 3, 5) represents the intrinsic lifetime of intermediate states 2, 3 and 5, σ is the absorption cross-section of the sensitizer of the excitation wavelength and $\rho(t)$ is the time dependent excitation power intensity function. ν is the excitation light frequency and h is Planck's constant, resonating with the transition of state $4 \rightarrow 5$. W_1 and W_2 represent the energy transfer rates of ETU1 and ETU2 between sensitizer and activator. Depending on the excitation function, this model can be applied to study static (*e.g.*, CW excitation) or dynamic systems (*e.g.*, pulsed excitation). These time resolved rate equations can be solved numerically or analytically, with each method having its pros and cons.

In the model reviewed above, the interaction between sensitizers, *e.g.*, CU, are not included, since it plays a trivial role compared to the dominating stepwise energy transfer in the system.[97,121–124] Nonradiative multiphonon relaxation (MPR) is included in this system in the overall decay constant (τ_2, τ_3, τ_5) of each state. These overall decay constants (τ_2, τ_3, τ_5) in the equations above can not be accurately determined directly through experiments and are instead often indirectly determined by theoretical calculations based on emission and absorption spectra.[125] The rate constants of the energy transfer rate W_1 and W_2 can be calculated by Kushida's theory based on Judd-Ofelt theory.[126]

Under Stokes excitation conditions, with GSA/ESA being the upconversion mechanism, the same energy structure as the standard two-photon model in Fig. 3.1 can be applied, but without any energy transfer process included. Solely through activator absorption resonating with incident photons, the activator is excited directly to the UCL state. The role of the sensitizer is limited and there is the possibility

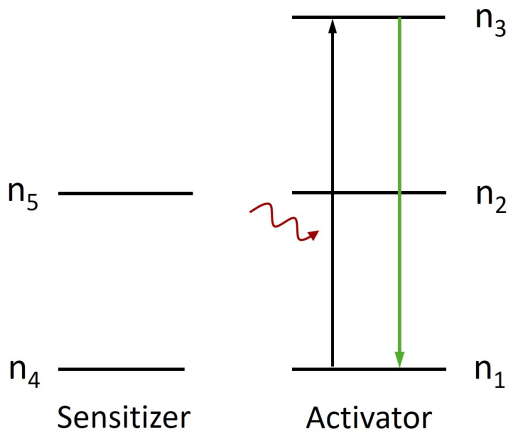

Figure 3.3: *GSA scheme with Stokes excitation.*

of energy back transfer from activator to sensitizer if the process is required to be considered in the model, *e.g.*, high sensitizer doping concentration or high surface related quenching. As illustrated in Fig. 3.3, only two processes are included in the system - direct excitation of the activator to the UCL state and direct radiative decay of the UCL state to the ground state.

This model can be representative for UCL emission with GSA/ESA being the upconversion mechanism, like direct excitation of Er^{3+} to the green UCL state through 485 nm excitation (paper II), direct excitation of Tm^{3+} to 808 nm emitting state through 795 nm excitation.[127] The time-dependent population of each energy state under Stokes excitation can be described in the equations below:

$$\text{State 1}: \frac{dn_1}{dt} = -\frac{\sigma_d \rho_d(t)}{h\nu_d} n_1 + \frac{n_3}{\tau_3}, \tag{3.9}$$

$$\text{State 3}: \frac{dn_3}{dt} = -\frac{\sigma_d \rho_d(t)}{h\nu_d} n_1 - \frac{n_3}{\tau_3}, \tag{3.10}$$

$$n_1 + n_3 = n_{\mathrm{A}}, \tag{3.11}$$

where ν_d is the frequency of the Stokes-excitation light, $\rho_d(t)$ is the time-dependent Stokes-excitation function, and σ_d is the absorption cross-section of the activator ions for the excitation of state $1 \rightarrow 3$. In this model, the kinetics of the UCL emitting state is solely decided by the excitation wave function and UCL intrinsic decay properties.

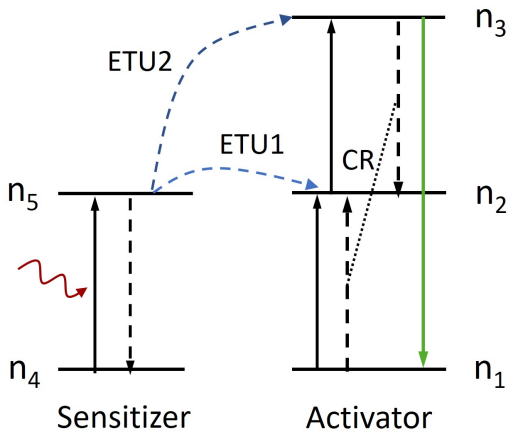

Figure 3.4: *Energy transfer upconversion (ETU) scheme with CR process involved for two-photon upconversion luminescence.*

3.3 Extended two-photon upconversion model

The models introduced in the last section do not include the CR through the Förster energy transfer process, which can occur between doped ions when the doping concentration is high or the excitation power density is high. Therefore, an extended two-photon upconversion model including the CR process can be introduced, as shown in Fig. 3.4.

Under high power intensity excitation and high activator doping conditions, the CR process can provide an extra decay channel for the UCL emitting state. It will lead to a faster decay speed, *i.e.*, shorter lifetime of this state. The corresponding time-dependent population of the first three equations (eqns. 3.3-3.5) in the standard two-photon upconversion model will then be modified into:

$$\text{State 1}: \frac{dn_1}{dt} = -W_1 n_5 n_1 - C n_1 n_3 + \frac{n_2}{\tau_2} + \frac{n_3}{\tau_3}, \tag{3.12}$$

$$\text{State 2}: \frac{dn_2}{dt} = W_1 n_5 n_1 + 2C n_1 n_3 - W_2 n_5 n_2 - \frac{n_2}{\tau_2}, \tag{3.13}$$

$$\text{State 3}: \frac{dn_3}{dt} = W_2 n_5 n_2 - C n_1 n_3 - \frac{n_3}{\tau_3}, \tag{3.14}$$

where C denotes the rate constant of the CR process. The extra CR-related component Cn_1n_3 is added into the first three rate equations of eqns. 3.3-3.5, with the rest eqns. 3.6-3.8 being the same.

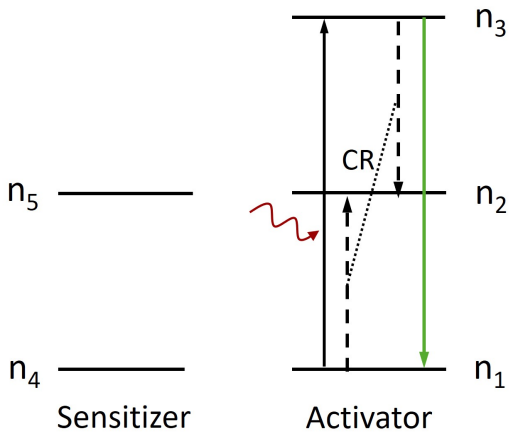

Figure 3.5: *GSA scheme with Stokes excitation with CR process involved for the two-photon upconversion luminescence*

The extended Stokes-excitation upconversion model including the CR process is illustrated in Fig. 3.5.

The time-dependent population density of each state including the CR process can then be described by the following equations:

$$\text{State 1}: \frac{dn_1}{dt} = -\frac{\sigma_d \rho_d(t)}{h\nu_d} n_1 - C n_1 n_3 + \frac{n_2}{\tau_2} + \frac{n_3}{\tau_3}, \tag{3.15}$$

$$\text{State 2}: \frac{dn_2}{dt} = 2C n_1 n_3 - \frac{n_2}{\tau_2}, \tag{3.16}$$

$$\text{State 3}: \frac{dn_3}{dt} = -\frac{\sigma_d \rho_d(t)}{h\nu_d} n_1 - C n_1 n_3 - \frac{n_3}{\tau_3}, \tag{3.17}$$

$$n_1 + n_2 + n_3 = n_{\mathrm{A}}. \tag{3.18}$$

In order to understand the UCL behaviour, simulations can be performed based on the rate equations formulated in the models mentioned above.

Although the theoretical methods are clear with including parameters that can give experimental interpretation, they obviously work under limited conditions. In some cases, it is difficult to obtain the derivation formula, like when the CR process is included. With numerical simulation methods one circumvents the difficulty of obtaining analytical solutions, and they may so have wider application, however, with the caveat that the affecting parameters are not appearing in an explicit way, which so can hamper the interpretation power.

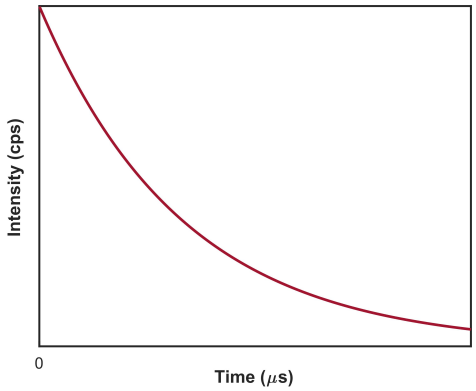

Figure 3.6: *Impulse response of sensitizer*

3.4 Theoretical derivation through UCL rate equations

In order to study the dynamic kinetics of UCL through time-dependent rate equations, a pulsed excitation can be applied as excitation stimuli. After such an external stimuli of short pulsed excitation, the differential equations applied to characterize the kinetics become non-linear and can not be solved analytically. To solve the rate equations of eqns. 3.3-3.8, some reasonable assumptions need to be applied. Under low power excitation and low doping concentration conditions, the upconversion process is seen as a minor kinetic perturbation, therefore $n_4(t)$ can be approximated to be a constant as the doping concentration of the activator n_S, n_1 is also constant and equals to the doping concentration of the activator after stimuli. Compared to $W_1 n_5 n_1$, $W_2 n_5 n_2$ is much smaller and can therefore be neglected in the equation. After a short pulse excitation, $\rho(t) = 0$ can be assumed and from eqn. 3.6, the formula

$$n_{5,\delta}(t) = n_5(0) e^{-\frac{t}{\tau_5'}}, \tag{3.19}$$

can be induced, where $\frac{1}{\tau_5'} = \frac{1}{\tau_5} + W_1 n_1$. τ_5' represents the effective lifetime of the sensitizer including radiative decay and nonradiative energy transfer to the activator and $n_5(0)$ is the population density at $t = 0$ right after the end of the excitation pulse. The time correlated intensity curve of the sensitizer will then show a monoexponantial decay behaviour with a time constant of τ_5', as shown in Fig. 3.6.

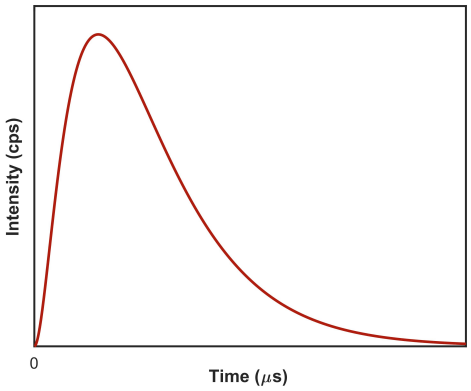

Figure 3.7: *Pulse response of UCL emitting state*

Through formula eqns. 3.3-3.8, the UCL emitting state of can be described as:

$$n_{3,\delta}(t) = \frac{W_1 W_2 n_1 n_5(0)^2}{\frac{1}{\tau_5'} - \frac{1}{\tau_2}}[(\frac{1}{(\frac{1}{\tau_2} + \frac{1}{\tau_5'} - \frac{1}{\tau_3})} - \frac{1}{(\frac{2}{\tau_5'} - \frac{1}{\tau_3})})e^{-\frac{t}{\tau_3}} + \frac{1}{(\frac{2}{\tau_5'} - \frac{1}{\tau_3})}e^{-\frac{2t}{\tau_5'}} + \frac{1}{(\frac{1}{\tau_2} + \frac{1}{\tau_5'} - \frac{1}{\tau_3})}e^{-t(\frac{1}{\tau_2}+\frac{1}{\tau_5'})}]. \tag{3.20}$$

The time correlated UCL intensity profile has three exponential components with time constants of $\frac{\tau_5'}{2}$, τ_3 and $\frac{1}{\frac{1}{\tau_2}+\frac{1}{\tau_5'}}$. Therefore, the curve is formulated by three parameters τ_5', τ_3 and τ_2 with $\frac{\tau_5'}{2}$, τ_3 as the decay parameters and $\frac{1}{\frac{1}{\tau_2}+\frac{1}{\tau_5'}}$ as the rising parameter. Therefore, the lifetime of the UCL emitting state is decided by the effective lifetime of the sensitizer, the intrinsic lifetime of the UCL emitting state and of the intrinsic lifetime of intermediate state. Compared to the simplified formula eqn. 3.1, there is one more extra decay component in the formula as there now are two pathways of depopulation of the UCL emitting state. When the difference between $\frac{\tau_5'}{2}$ and τ_3 is significant, then basically the much larger decay parameter is deciding the decay speed. That is to say, if the intrinsic lifetime of the UCL emitting state, τ_3, is much larger than half of the sensitizer effective lifetime, the fitted parameters τ_d and τ_r can represent the intrinsic lifetime τ_3 and the rise parameter of $\frac{1}{\frac{1}{\tau_2}+\frac{1}{\tau_5'}}$ when fitting the profile with two exponential components. If the opposite situation, $\tau_5'/2 \gg \tau_3$, is the case, then interpreting the τ_d as the intrinsic lifetime of the UCL emitting state is not accurate, in fact it then represents $\frac{\tau_5'}{2}$. If the values of $\tau_5'/2$ and τ_3 are similar, then the interpretation of τ_d and τ_r as intrinsic lifetime and rise time could both be inaccurate.

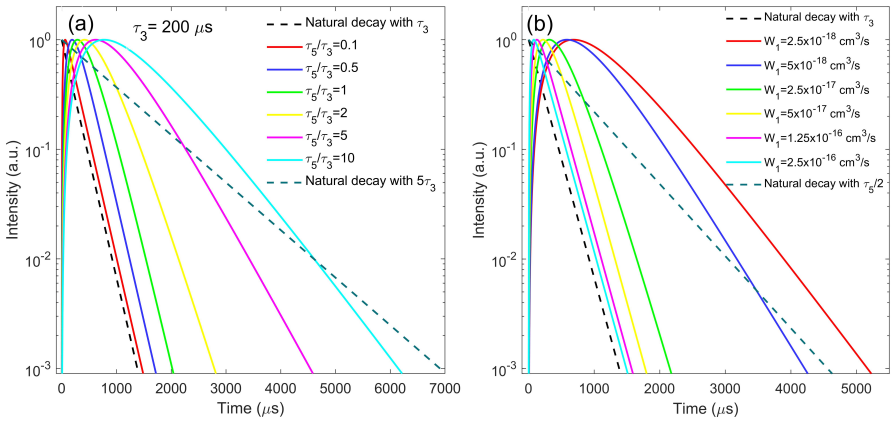

Figure 3.8: *Simulated UCL state population n_3 decay profile under short pulsed excitation a) with different τ_5/τ_3, b) with different W_1 (from paper II). Copyright 2019, The Royal Society of Chemistry.*

3.5 Numerical simulations of UCL rate equations

Even though analytical derivations from rate equation models often are straightforward to exhibit IRF with clear affecting parameters, numerical simulation methods can be a powerful supplementary method when inducing analytical derivations is difficult. By numerical simulations, parameters affecting the kinetics of the UCL can be studied with results exhibited in a graphical way, instead of formulaic way. For example, the influence of the lifetime of the intermediate states on UCL emitting kinetics based on the model shown in Fig. 3.1a has been systematically studied (paper II) with time constant parameters chosen appropriately from literature. The numerical simulation results show a similar result as from eqn. 3.20, which is demonstrated in Fig. 3.8.

The time correlated UCL intensity profiles also exhibit dependence on the parameters - ETU energy transfer rate, W_1, and radiative lifetime of sensitizer τ_5 - which together determine the effective lifetime of the sensitizer (τ_5'). The decay profile is co-determined by both the intrinsic lifetime τ_3 and the effective lifetime of the sensitizer, with the larger one mainly deciding the decay profile. When W_1 increases, or sensitizer radiative lifetime τ_5 decreases, the effective lifetime will decrease. As a result, the intrinsic lifetime of the UCL emitting state becomes much larger than the effective lifetime of the sensitizer and starts to dominate the decay profile.

With numerical simulations, the influence of the CR process between the activator ions on the UCL emitting behaviour given by the standard two-photon upconver-

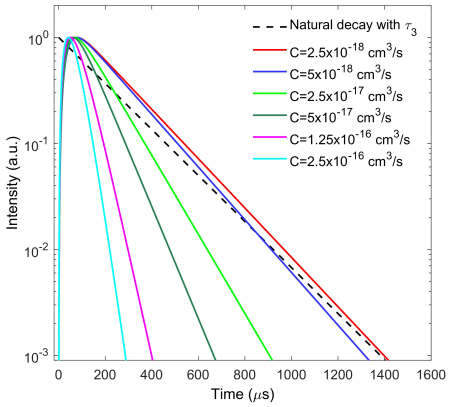

Figure 3.9: *Simulated UCL state population n_3 decay profile under short pulsed excitation with different CR coefficient C (from paper II). Copyright 2019, The Royal Society of Chemistry*

sion model can be studied. With ETU being the main upconversion mechanism, the CR process would lead to a faster decay of the UCL emitting state, which is predictable. With alrger CR coefficients, the UCL decays faster. Fig. 3.9 exhibits a simulation of the influence of the CR coefficient on the decay speed of the UCL emitting band. Other factors affecting decay speed, including excitation power density and CR processes between sensitizers, can also be studied with numerical simulations.

Considering numerical simulation results, we can understand that the decay speed is affected by many factors, including the CR process, the ETU energy transfer rate between sensitizer and activator, etc. This leads to the question of the validity to extract an intrinsic lifetime of the UCL emitting state from the time-correlated UCL intensity curve under anti-Stokes excitation conditions. As discussed above, it is the PL temporal comprehensive response of the whole UC system to the excitation function instead of the intrinsic lifetime the UCL emitting state that matters. Generally, Stokes excitation is preferred to obtain the intrinsic lifetime, even though cross-relaxation between sensitizers could also complicate the decay properties and make the measurements invalid to some extent (paper III).

Chapter 4

The response of UCL to temporally extended excitation

4.1 Introduction

Even though basic theories have been established to study UCL kinetics, there are still strong theoretical challenges to battle in order to predict and explain UCL behavior. The rate equation models have been commonly applied in studies of UCL mechanisms for analytical and numerical simulations.[116,128] Such simulations have many advantages and the most important ones are that they can be applied to predict the behavior of UCL, such as QY,[73] relative intensity ratios of emission bands,[116] effects of doping concentration,[30] effect of excitation power density.[30] For example, the upconversion mechanism of Yb^{3+}, Tm^{3+} co-doped $NaYF_4$ has been reported by many studies, but due to lack of substantial experimental evidence, the uncertainties regarding photophysical kinetics, like the PA mechanism, still remain. Therefore, rate equation models have been applied to study the temporal evolution of PA behavior of 808 nm emission in the system, *e.g.*, by Hossan *et al.*[116]

Varying the excitation function, the UCL time correlated profile changes correspondingly, leading to varied properties like: overall color output due to change of intensity ratio among UCL bands and upconversion mechanisms. Therefore, to understand the UCL kinetics under different excitation functions using simulations is crucial. In this chapter, the impulse response of the UCL emitting state obtained from both analytical and numerical simulations are introduced. The response of UCL to temporally extended excitation, *i.e.*, square wave function, will so be discussed. Inspired by the square wave excitation response properties of UCL, emerging applications of UCNPs for optical encoding, using the advantages of the pulse duration response of square wave excitation, are presented.

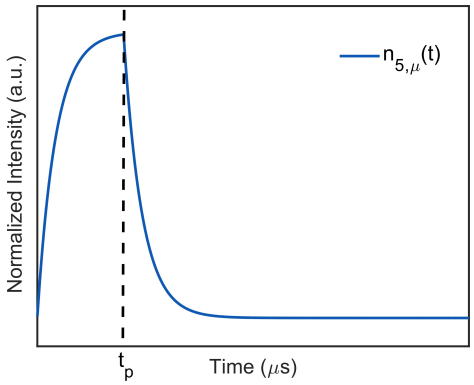

Figure 4.1: *Square wave response of sensitizer excited state* $n_{5,\mu}(t)$.

4.2 Excitation duration response

The ideal excitation function is a $\delta(t)$ function with infinite short pulse duration. The corresponding IRF is introduced as in eqn. 3.20 from chapter 3 based on the standard two-photon model described in Fig.3.1. In the real case, the excitation wave function width t_p is not infinitely small, therefore, the result will be a convolution of the IRF and the excitation function. When a square wave excitation with pulse duration of t_p and period of T is introduced, the excitation function reads as follows:

$$\mu(t) = \begin{cases} 1, & t < t_p \\ 0, & t > t_p \end{cases} \tag{4.1}$$

The sensitizer excited state response function will then be the convolution of IRF $n_{5,\delta}(t)$ as in eqn. 3.19 with the square-wave excitation function:

$$n_{5,\mu}(t) = \mu(t) \circledast n_{5,\delta}(t). \tag{4.2}$$

The result formula reads as expressed below:

$$n_{5,\mu}(t) = \begin{cases} \alpha(1 - e^{-\frac{t}{\tau_5'}}), & t < t_p \\ \alpha e^{-\frac{t}{\tau_5'}}(e^{-\frac{t_p}{\tau_5'}} - 1), & t_p \leq t < T \end{cases} \tag{4.3}$$

where $\alpha = n_{5,\delta}(0)\tau_5'$. An illustration curve for the sensitizer state $n_{5,\mu}(t)$ is shown in Fig.4.1.

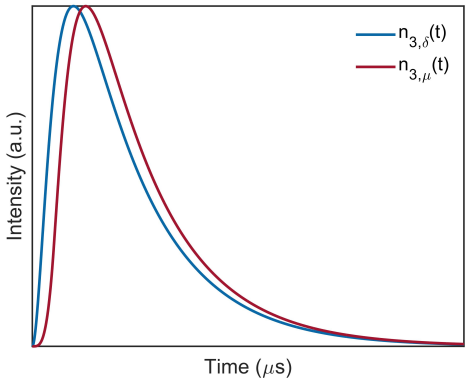

Figure 4.2: *Impulse response and square wave response of the UCL emitting state population.*

In the same way as we deduced the impulse response of UCL emitting state $n_{3,\delta}(t)$, $n_{3,\mu}(t)$ can be deduced from the rate equations of eqns. 3.3-3.8 - the formula is shown below:

$$n_{3,\mu}(t) = \begin{cases} M\{A + Be^{-k_3 t} + Ce^{-k_2 t} + De^{-k_5 t} + Ee^{-2k_5 t} + Fe^{-(k_5+k_2)t}\}, t < t_p, \\ Me^{-k_3 t}\{G(t_p) + H(t_p)[g(t_p)(e^{(k_3-k_2-k_5)t} - e^{(k_3-k_2-k_5)t_p}) \\ \qquad\qquad + f(t_p)(e^{(k_3-2k_5)t} - e^{(k_3-2k_5)t_p})]\}, t_p \leq t < T, \end{cases} \tag{4.4}$$

where $M = W_2 W_1 n_1 (n_5(0)\tau_5')^2$, and A, B, C, D, E and F are constants decided by $k_2 = \frac{1}{\tau_2}$, $k_3 = \frac{1}{\tau_3}$ and $k_5 = \frac{1}{\tau_5'}$. $G(t_p), g(t_p), f(t_p)$ are functions decided by the k_2, k_3 and k_5 parameters and by the square wave pulse duration t_p. The profile is thus still co-determined by parameters of τ_5', τ_3 and τ_2 and also one more parameter, pulse duration t_p. The time correlated curve is similar to the IRF with rise and decay profiles but with delayed maximum intensity. As shown in Fig. 4.2.

The longer the pulse duration is, the more the profile will shift to the right. When the pulse duty cycle $\frac{t_p}{T}$ is very small, less than 1%, the profile shift is negligible and the square-wave response can be regarded as an impulse response to extract the time constants parameters. After a pulsed square wave excitation with duration of t_p, the total emitted UCL photons within one period of time, T, can be obtained by integrating the curve over the whole period of time, and the result formula will be:

$$F(t) = \int_0^T n_{3,\mu}(t) d\tau. \tag{4.5}$$

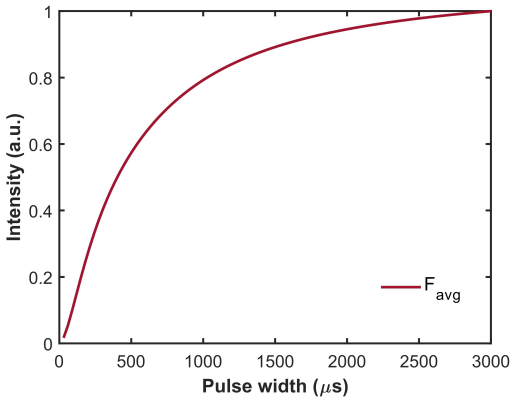

Figure 4.3: *UCL intensity over one period.*

The averaged luminescent intensity over pulse duration t_p is then described as:

$$F_{avg}(t) = \frac{F(t)}{t_p}. \tag{4.6}$$

Eqn. 4.6 is pulse duration dependent. The averaged UCL intensity-pulse duration curves are illustrated in Fig.4.3

Another way to analytically solve the UCL time correlated rate equations is through a Laplace transform only assuming $n_4 = n_S$ and $n_1 = n_A$. Then during and after the pulse excitation $\rho(t)$, the sensitizer excited state n_5 population can be expressed as:

$$n_5(t) = \frac{\sigma}{h\nu} n_4 \rho(t) \circledast e^{-\frac{t}{\tau_5'}}. \tag{4.7}$$

Depending on the excitation function $\rho(t)$, the convolution result of the formula will change. If the excitation is an ideal short pulse excitation, $\rho(t) = \delta(t)$, then the reduced formula function is the IRF similar to eqn. 3.20. If the excitation is a square wave excitation, $\rho(t) = \mu(t)$, the reduced sqaure-wave response result is similar to the result in eqn. 4.4.

4.3 Pulse duration response of PL color output

Due to the different rise and decay times, the population of UCL emitting bands are built up to different levels within the same time when excited with a square wave pulsed excitation. As a result, the overall color output varies with the pulse duration as is shown in Fig. 4.4.

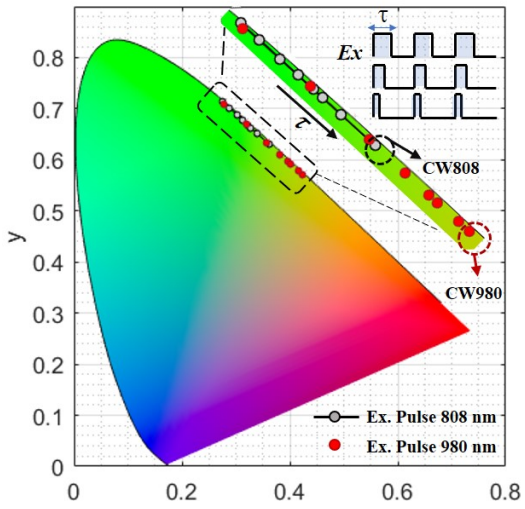

Figure 4.4: *CIE color output change corresponding to pulse duration τ (from paper I). Copyright 2019, Elsevier.*

In the figure we see that, under either 808 nm or 980 nm excitation, with the pulse duration changing from 18 μs to 279 μs the output color varies from green to yellowish due to the different building up and decay times of the green (525/540 nm) UCL emitting band and the red (654 nm) UCL emitting band of Er^{3+}. With this ability to tune the dynamic color output, UCNPs can be applied for dynamic optical imaging for anti-counterfeiting, or optical encoding, taking advantage of the pulse duration response property. For example, Han's group applied pulse duration of 100 μs, 500 μs and 6000 μs with an identical period of 10 ms.[129] and could show that the color output of $NaYF_4$:Er^{3+}/Tm^{3+}@$NaYF_4$ nanoparticles changes from green to yellow and to red.

4.4 From experimental regulation of temporal response to optical encoding applications of UCNPs

As we discussed before, UCNPs have gained a lot of attention for optical encoding. Even though many optical encoding dimensions of UCNPs have been studied, discovering more dimensions can always be encouraged as they are beneficial. Due to the benefits of dynamic encoding with larger information store capacity, the pulse duration response of UCL has been considered as a new optical encoding dimension (paper V). Through the pulse duration response dimension, the averaged UCL intensity over the pulse duration time can be applied as a dynamic optical

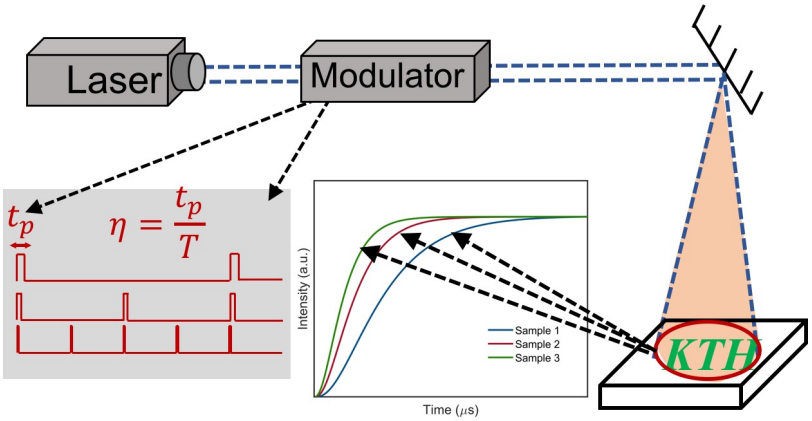

Figure 4.5: *Schematic illustration of the setup and principle of pulse duration response optical decoding.*

encoding approach, as described in eqn. 4.6. Through the experimentally obtained $F(t_p)$ *vs* t_p curve, the parameters τ_3, τ_5' and τ_2 in eqn. 4.6 can be extracted by fitting the curve with the formula. These parameters can then be applied as a decoding dimension to distinguish different samples for encoding purpose. With the three parameters as a distinguished dimension, the encoding capacity can be sharply enhanced together with other dimensions, *e.g.*, color. Applying the modulated periodic excitation with varied pulse duration, the total luminescent state population of the printed pattern can be recorded by a CCD camera within an experimental time scale of seconds. The total luminescent state population can then be divided by camera exposure time to obtain the time-averaged luminescent state population, $F(t_p)$, for each pattern region, as illustrated in Fig. 4.5. With this method, no fast speed scan camera is needed for decoding, which makes it easier to access. It is to be noted that the duty circle of pulse, $\eta = \frac{t_p}{T}$, should be set low to make sure that the luminescent state relaxes to the ground state before the onset of next pulse and to avoid saturation effects.

4.5 From experimental regulation of temporal response to NIR photodetector applications of UCNPs

UCNPs have been applied for NIR photodetector light receivers as reported in many works.[110,130–132] NIR photodetectors are able to detect multiple bands within NIR, simultaneously. Therefore, it is momentous to discriminate the wavelength of the incident light for selective multispectral photodetectors. Due to the response time of the UCL emitting state, the emission intensity of UCL differs under varied

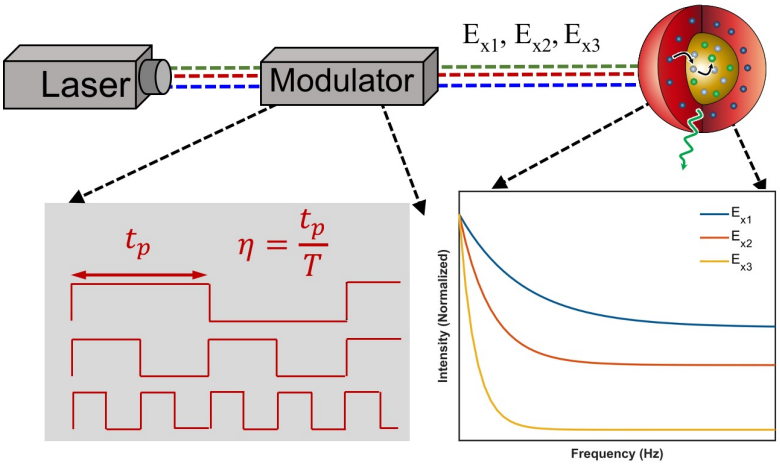

Figure 4.6: *Schematic illustration of modulation frequency response for selective multispectral NIR photodetection.*

frequency excitation with same duty cycle. Since under different wavelength excitations, the UCL intensity change varies corresponding to varied excitation light frequency, and the changing rate can be applied as a distinguish factor to differentiate excitation wavelengths. *e.g.*, to distinguish among 808 nm, 980 nm or 1540 nm excitations of sample $NaYF_4$: Yb^{3+}, Er^{3+}@$NaYF_4$@$NaYF_4$:Yb^{3+}, Nd^{3+}, Tm^{3+} (paper IV). Moreover, with this novel approach, even under mixed excitation with several bands (*e.g.*, 808 nm, 980 nm and 1540 nm together), the percentage of each excitation intensity can be determined by the same changing rate *vs* pulse frequency correlation, as schematically illustrated in Fig. 4.6. Through this way, the UCL band distinguishable ability of photodetectors can stimulate other applications of upconversion nanotechnology.

Chapter 5

Excitation light intensity response of UCNPs

5.1 Introduction

Owing to the property of two or multiple photons absorbance to produce UCL, the UCL intensity exhibits a nonlinear power dependence. It is essential to understand this intensity dependence on power density for a better understanding of the upconversion mechanism and for advancing the applications of UCNPs. A lot of work has been devoted to the investigation of power density dependence of photoluminescence, like Pollnau *et al* and many other groups who have systematically studied the power density dependence of upconversion luminescence at steady state through simplified rate equations.[55,56] The power density could impose restriction on the applications of UCNPs. For example, for bioimaging applications, the nonlinear power density dependence can result in dramatic signal reduction at deep tissue ($\sim$1 cm).[133] For photovoltaic device sensitization, high power density of excitation is usually needed (>1 W/cm^2), which is much higher than the solar irradiance intensity (0.1 W/cm^2).[17,18] In the meanwhile, the UCL power density dependence can be explored to determine the upconversion mechanism and extend applications like multicolor imaging. Therefore, in this chapter, the UCL power density dependence will be discussed in detail and also various applications corresponding to the power density dependence will be introduced.

5.2 Power density dependence of UCL

5.2.1 UCL power density response

Based on the standard two-photon upconversion model described in chapter 3, eqn. 3.3-3.8 and Fig. 3.1, rate equations under steady state are shown below:

$$\text{State } 2: \frac{dn_2}{dt} = W_1 n_5 n_1 - W_2 n_5 n_2 - \frac{n_2}{\tau_2} = 0, \tag{5.1}$$

$$\text{State } 3: \frac{dn_3}{dt} = W_2 n_5 n_2 - \frac{n_3}{\tau_3} = 0, \tag{5.2}$$

$$\text{State } 5: \frac{dn_5}{dt} = \frac{\sigma\rho(t)}{h\nu} n_4 - \frac{n_5}{\tau_5} = 0, \tag{5.3}$$

$$n_1 = n_{\mathrm{A}}, \tag{5.4}$$

$$n_4 = n_{\mathrm{S}}. \tag{5.5}$$

In this model, the depletion of the ground state of sensitizer 4 and activator 1 is not considered and the sensitizer ETU rate is not included for depopulation of the sensitizer excited state 4 assuming its linear decay is much faster than the ETU process. The power density dependence of the UCL emitting state can be described as:[58]

$$I_{\mathrm{em}} = \frac{n_3}{{\tau_3}^{rad}} = \frac{\alpha\rho^2}{\beta + \gamma\rho}, \tag{5.6}$$

where $\alpha = W_1 W_2 \tau_5 (\tau_3/{\tau_3}^{rad}) n_1 {n_4}^2 (\sigma/h\nu)^2$, $\beta = \frac{1}{\tau_2}$ is the linear decay of state population n_2, including both radiative and nonradiative pathways, and $\gamma\rho = W_2\tau_5(\sigma/h\nu)\rho$ is the ETU rate of n_2. Under low power density excitation, the linear decay of state population n_2 is much bigger than the ETU rate, $\beta \gg \gamma\rho$, leading to a quadratic dependence of the UCL intensity on power density, *i.e.*, $I_{\mathrm{em}} = \frac{\alpha\rho^2}{\beta}$. Under high power excitation, the linear decay of state n_2 is dominated by the ETU rate and leads to a linear power density dependence of the UCL intensity, *i.e.*, $I_{\mathrm{em}} = \frac{\alpha\rho}{\gamma}$. The slope factor n of $logI$ over $log\rho$ can then be represented as:[58]

$$n = \frac{dlogI}{dlog\rho} = 1 + \frac{1}{1 + \tau_2 W_2 \tau_5 \sigma n_1 \rho}, \tag{5.7}$$

and n is the value for a standard two-photon upconversion process and varies in the range 2 to 1.

For a standard three-photon upconversion model depicted in Fig. 5.1, the rate equations under steady state are listed below:

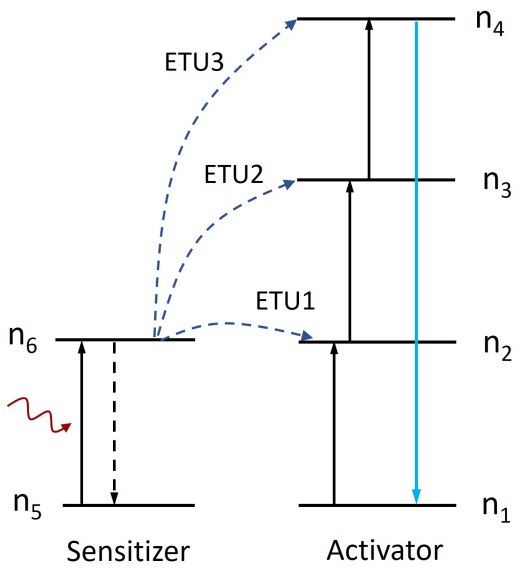

Figure 5.1: *A standard three-photon upconversion model.*

$$\text{State 2}: \frac{dn_2}{dt} = W_1 n_6 n_1 - W_2 n_6 n_2 - \frac{n_2}{\tau_2} = 0, \tag{5.8}$$

$$\text{State 3}: \frac{dn_3}{dt} = W_2 n_6 n_2 - W_3 n_6 n_3 - \frac{n_3}{\tau_3} = 0, \tag{5.9}$$

$$\text{State 4}: \frac{dn_4}{dt} = W_3 n_6 n_3 - \frac{n_4}{\tau_4} = 0, \tag{5.10}$$

$$\text{State 6}: \frac{dn_6}{dt} = \frac{\sigma\rho(t)}{h\nu} n_5 - \frac{n_6}{\tau_6} = 0, \tag{5.11}$$

$$n_1 = n_A, \tag{5.12}$$

$$n_4 = n_S. \tag{5.13}$$

The depletion of sensitizer and activator ground state is neglected and the linear decay is considered to be much faster than the ETU process of state 6. As a result, the state 6 density n_6 is represented as:

$$n_6 = \frac{\sigma\rho}{h\nu} n_5 \tau_6, \tag{5.14}$$

and the UCL intensity n_4 of state 4 is represented as:

$$I_{\text{em}} = \frac{n_4}{{\tau_4}^{rad}} = \frac{\tau_4}{{\tau_4}^{rad}} \frac{W_1 W_2 W_3 n_1 (n_6)^3}{(W_3 n_6 + \frac{1}{\tau_3})(W_2 n_6 + \frac{1}{\tau_2})}. \tag{5.15}$$

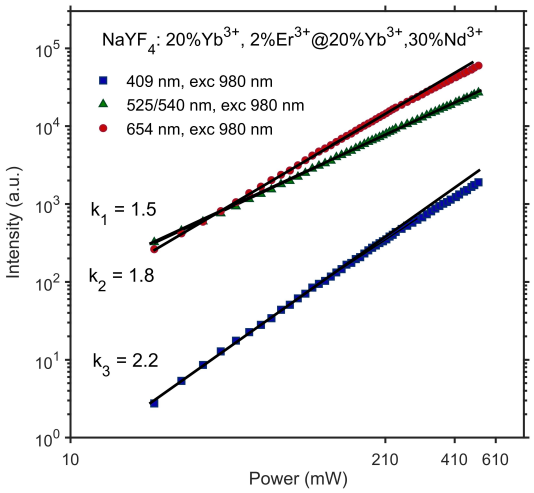

Figure 5.2: *Power density dependence of blue (409 nm), green (525/540 nm) and red (654 nm) UCL bands under CW 980 nm excitation (from paper III). Copyright 2019, The Royal Society of Chemistry.*

Under low power excitation, the ETU rates of states 2 and 3 are much slower than the linear decay rates, respectively, leading to $\frac{1}{\tau_3} \gg W_3 n_6$ and $\frac{1}{\tau_2} \gg W_2 n_6$. As a result, $I_{\text{em}} = k{n_6}^3 \propto \rho^3$. The UCL intensity shows a cubic dependence on the power density. Under high power density, $I_{\text{em}} = k_1 n_6 \propto \rho$, thus showing a linear power dependence. Then the slope factor n of $logI$ over $log\rho$ changes within values of 3 to 1. Therefore, the slope factor n of $log(\rho)$-$log(I_{\text{em}})$ curve obtained experimentally at low power density can be applied to determine the upconversion mechanism. If the underlying upconversion mechanism are the GSA, ESA and ETU mechanisms, the slope factor n equals to the number of photons absorbed to emit one upconverted photon under low power density excitation and gradually decreases to 1 with power increased. In the meantime, for real UCL measurements, the upconverting mechanism is more complicated, and additional processes, *e.g.*, CR between excited ions under high doping conditions, or ground state depletion under high power density, may play non-negligible roles. As a result, the slope factor of n could show abnormal values in the measurement and can even be smaller than 1.[56]

As an example of applying power density dependence to study an upconversion mechanisms, Fig. 5.2 presents the power density dependence of UCL under CW excitation of core-shell $NaYF_4$:Yb^{3+},Er^{3+}@$NaYF_4$:Yb^{3+},Nd^{3+} nanoparticles. In Fig. 5.2, all of the ETU emitting bands, green (525 nm/540 nm), red (654 nm) and blue (409 nm), exhibit a power density dependence at CW 980 nm excitation,

featuring a slope factor of 1.5, 1.8 and 2.2 at low excitation intensity. Through the slope value, green emission can be interpreted as a two-photon upconverison mechanism and the blue emission as a three-photon upconversion mechanism. The red emission upconversion mechanism is more complicated than being fed by the green emitting state through nonradiative relaxation since the power density dependence slope is apparently higher than of the green emission. Higher order multiphoton processes beside the two-photon upconversion pathway for red emission is indicated as has been discussed in many reported studies.[134,135] With power density increased, the excitation intensity dependence becomes less dominant and shows a saturation effect due to competition between the natural radiative decay and the nonradiative ETU processes.[55,56,73] These are examples that from the power density dependence curve the upconversion mechanism can be investigated to some extent. It should be noted that due to saturation effect at high power, it is required that the power density dependence profile is obtained under low power in order to interpret the upconversion mechanisms more precisely.

5.2.2 Quantum yield power density dependence

Due to the power density dependence of UCL, it is difficult to compare among reported works based on UCL intensity. The QY is nowadays applied as a criterion to compare among the reported studies. Due to the nonlinearity of UCL, the QY of UCNPs shows power density dependence, with a higher QY at a higher power density. To numerically solve the rate equations described before in chapter 3 and 4 at steady state, by choosing parameters carefully the QY can be derived precisely in principle. An analytical expression of the QY derived from rate equations under steady state, thus from eqn. 5.2-5.5, can be easily obtained as a valuable reference for the standard two-photon upconversion model described in chapter 3, see Fig. 3.1. The correlation between QY, Φ_{2-ph}, of the two-photon UCL emitting state 3 and excitation intensity (ρ) is described in the formula below:[73]

$$\Phi_{2-ph} = \frac{I_{\mathrm{em}}}{\sigma \rho n_4} = \frac{\Phi_s \rho}{\rho_b + \rho}, \tag{5.16}$$

where $\Phi_s = W_1 n_1 \tau_5 (\tau_3 / {\tau_3}^{rad})$ is the maximum QY that the two-photon UCL can achieve, which is the saturation level when the natural decay pathway of the UCL emitting state is dominated by energy transfer. ρ_b is the balancing excitation intensity, which when QY equals to half of Φ_s - $\rho_b = \rho_{(\mathrm{QY}=\Phi_s/2)}$. Thus given the same amount of photons, a higher excitation intensity would lead to a larger number of upconverted photons. Numerically solving the equation eqn. 5.16, the correlation described by the formula above is plotted in Fig. 5.3

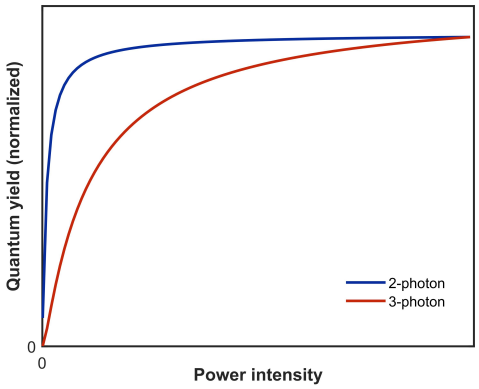

Figure 5.3: *Quantum yield power density dependence of two-photon and three-photon upconversion systems.*

For standard three-photon upconversion model, the QY is represented as:

$$\Phi_{3-ph} = \frac{I_{\text{em}}}{\sigma\rho n_5} = \frac{\Phi_s \rho^2}{(\rho_{b1}+\rho)(\rho_{b2}+\rho)}, \tag{5.17}$$

where $\Phi_s = W_1 n_1 \tau_6 (\tau_4/{\tau_4}^{rad})$ is the saturation QY when the linear decay of state 3 and state 2 both can be neglected. $\rho_{b1} = \frac{h\nu}{\tau_2 n_5 \tau_6 W_3 \sigma}$ is the balancing excitation intensity when the linear decay of state 2 equals to the ETU rate of state 2 and $\rho_{b2} = \frac{h\nu}{\tau_2 n_5 \tau_6 W_2 \sigma}$ is the balancing excitation intensity when the linear decay and ETU rate of state 3 are equal. The correlation described in eqn. 5.17 is illustrated in Fig. 5.3, showing that the QY of the three photon process reaches saturation slower than two photon process.

5.2.3 Power density dependence of PL color output

The intensity ratio among UCL emitting bands is sensitive to the power density. As a result, the same UCNPs can exhibit different color outputs corresponding to power excitation conditions. Fig. 5.4 exhibits the CIE chromaticity coordinates of core-shell $NaYF_4$:Yb^{3+}, Er^{3+}@$NaYF_4$:Yb^{3+}, Nd^{3+} nanoparticles, when subject to either CW 980 nm or CW 808 nm excitation with different power intensities.

Xue *at al*[136] showed that with increasing power density, the UCL color output can change from green to yellowish, with the color span of 808 nm excitation being much smaller than that of 980 nm excitation. This is due to the asynchronized power dependence of different emission bands between 808 nm and 980 nm excitations. This creates a dimension for dynamic optical imaging applications.

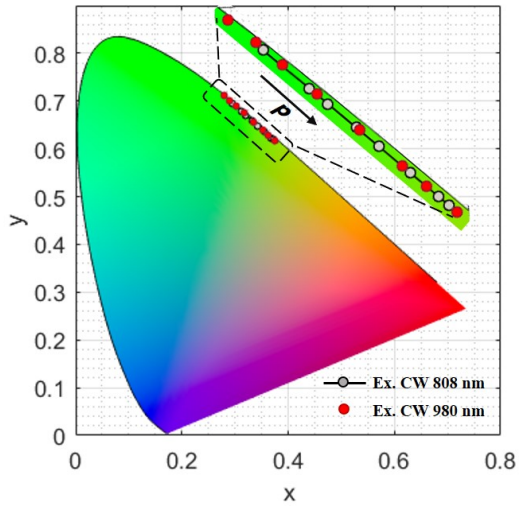

Figure 5.4: *CIE chromaticity coordinates of the core-shell $NaYF_4$:Yb^{3+}, Er^{3+}@$NaYF_4$:Yb^{3+}, Nd^{3+} nanoparticles under either CW 808 nm or CW 980 nm excitation (from paper I). Copyright 2019, Elsevier.*

5.3 UCL enhancement of UCNPs

Under low power density, the UCL intensity is weak. As a result, the applications of UCNPs requiring high UCL intensity are restricted. To enhance UCL intensity is thus crucial to make UCNPs-related applications practical. The ways to enhance UCL are categorized into groups: to enhance absorption,[137,138] to increase QY,[139] to suppress non-radiative loss.[41] All three ways have been well explored by many works. Here two popular methods at heat are introduced, *i.e.*, to enhance absorption with plasmonic effects and increase QY with light concentrators.

5.3.1 UCL enhancement with light spatial modulator

Light spatial modulators, as light concentrators, have been introduced for UCNPs-related applications like solar cells, organic LEDs, sensors, microsystems by some reported work.[140–145] Light concentrators, as light collecting layers, have the advantages to increase the light harvesting angle, reduce light reflection and prolong the light propagation path length. Under low power density irradiance, light modulators can enhance incident light intensity and increase the QY sharply. Under high power excitation, the enhancing ability of light modulators can be limited due to saturation effects. Compared with plain bulk materials, like plain solar collecting films, periodic-structured materials can interact with light in more adjustable and sophisticated ways that can serve as a new platform. Microlens array

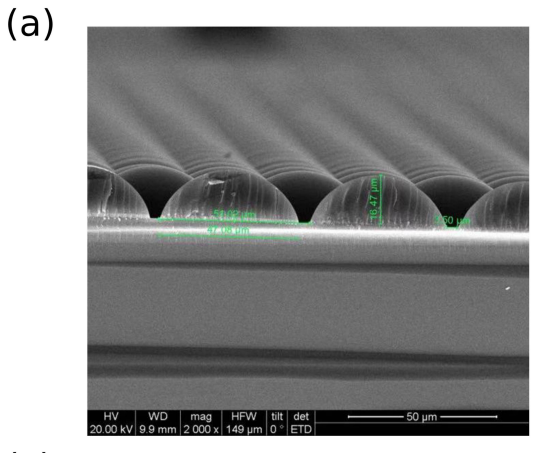

Figure 5.5: *Scanning Electron Microscopy (SEM) image of microlens array (from paper III). Copyright 2019, The Royal Society of Chemistry.*

(MLA) with microscale size and periodic structures used as light concentrators have been reported in many works.[141–144] MLA can be fabricated through low-cost and low-loss approaches, *i.e.* photolithography with photoresists, with the optical layer produced by cheap materials like polymethylmethacrylate (PMMA) or fused silica with high transparency and small light loss. Through design of the contact angle of lens with substrate, the lens size (nm to μm), the lens shape (e.g. hexagonal, spherical, plano-convex and cylindrical), the lens array packing arrangement (e.g. rectangular packed, hexagonal packed) and the interspace distance, makes it possible to flexibly modify the performance of microlens arrays as light spatial modulators.

As an example, Fig. 5.5 exhibits a SEM image of a microlens array with plano-convex shaped quartz microlenses on a polycarbonate substrate.

By concentrating the excitation light to increase the power density with MLA, the QY can be enhanced especially under low excitation intensity conditions due to the QY power density dependence. As the UCL emitting intensity (I_{em}) is proportional to the nth of power density (ρ), *i.e.* $I_{\mathrm{em}} \propto \rho^n$. The enhancement ability of MLA is dependent on the excitation power density. Under low power density, the slope value n is bigger, leading to a bigger value of $\delta(I_{\mathrm{em}}) = {\rho_1}^n - {\rho_0}^n$, *i.e.*, and a bigger UCL enhancement. Therefore, under solar irradiation (0.1 W/cm^2), MLA works better than under high power excitation, which is beneficial for solar cell sensitization. As illustrated in Fig. 5.6, the UCL enhancement ability of the 450 nm emitting band of sample $NaYF_4$:Yb^{3+}, Tm^{3+}@$NaYF_4$:Yb^{3+} decreases with increasing the power. MLA has experimentally been proven to give an UCL en-

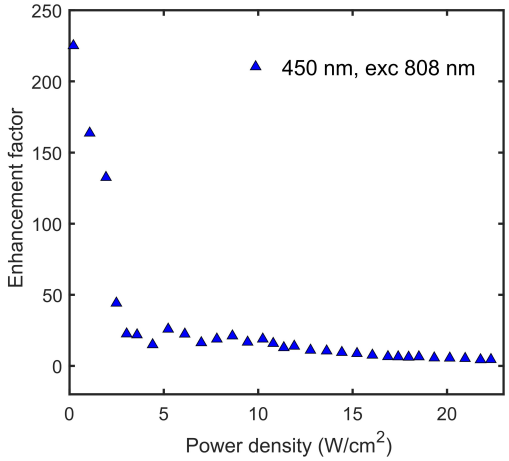

Figure 5.6: *Power density dependence of the microlens array enhancement factor of the 540 nm UCL emitting band of core-shell $NaYF_4$:Yb^{3+}, Tm^{3+}@$NaYF_4$:Yb^{3+} under CW 808 nm excitation (from paper III). Copyright 2019, The Royal Society of Chemistry.*

hancement factor of 2 to 3 orders of magnitude, as shown in paper IV of the thesis. The modification ability of MLA can be investigated through optical simulations to study and predict the UCL MLA enhancement ability. It could be a practical guidance for PL performance investigations. The use of the software Zemax for ray tracing simulations has been reported by several works on MLA.[141,146,147] Through ray tracing simulations, the focal point of the MLA can be adjusted and the placing of the UCNPs at the focal point can be guided to maximize the PL enhancement. Through simulations, the affecting parameters, e.g. lens density, lens size and shape, lens contacting angle, can all be studies theoretically to modify the performance of MLA to maximize the PL enhancement ability. Fig. 5.7 is an example of ray tracing simulations with Zemax. The light distribution before and after MLA are detected and shown in Fig. 5.7a and Fig. 5.7b, respectively. The ratio of the integrated UCL intensity between the plane Fig. 5.7b/Fig. 5.7a then defines the PL enhancement factor. By choosing a proper value of the power density dependence factor n, the enhancement of each UCL emitting band can be predicted.

5.3.2 DSSC efficiency enhancement through use of MLA&UCNPs

Thanks to recent advances in upconversion nanochemistry, high quality UCNPs with a high luminescent QY up to 10.5% and above can be achieved at power

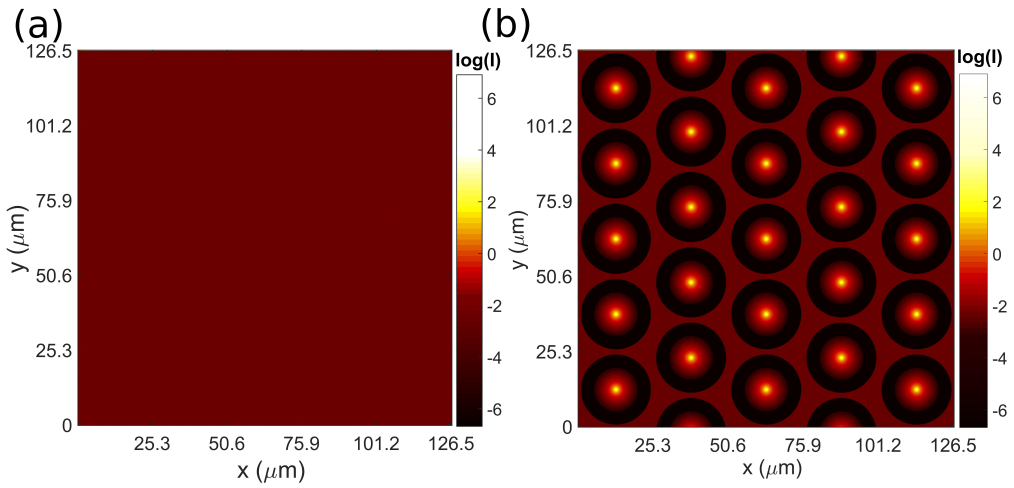

Figure 5.7: *Simulation of excitation light distribution before MLA (a) and after (b) MLA (from paper III). Copyright 2019, The Royal Society of Chemistry.*

density of 30 W/cm^{-2}.[70,148] Due to the QY power density dependence as described above, to achieve this high QY, a high power density typically well above 1 W/cm^2 is required. This power density is much higher than the IR density in the sun irradiance (1.5 M, 100 mW/cm^2). Therefore, when incorporated into solar cells, the contribution of UCNPs to solar cell efficiency is negligible under regular sun irradiance.[73] Therefore, some extra steps are needed to enhance the UCNP QY in order to make UCNP sensitized solar cells practical. As discussed in the section above, MLA has the ability to significantly enhance the PL of UCNPs. A strategy to improve solar cell efficiency by UCNPs assembled together with MLA can be applied to sensitize dye sensitized solar cells (DSSCs) to study the enhancement ability of UCNPs on solar cells efficiency taking advantage of the nonlinearity of UCNPs. The proposed strategy can overcome the high excitation intensity threshold of UCNPs and bring about future breakthrough in energy applications. MLA can be easily integrated into photoic devices. In addition, the availability of relatively low cost raw material with transparency above 95% (*e.g.*, polymers) and fabricating techniques potentially makes the cost affordable for large-scale production. As is shown in Fig. 5.8, a strategy to assemble MLA and UCNPs to sensitize DSSCs together can readily be practised.

Through the strategy reviewed above, the overall DSSC efficiency is improved by a percentage of 6.15% with UCNPs and MLA compared with solely an UCNP-enhanced DSSC, and an overall 9.51% enhancement compared with a control DSSC cell (without UNCP nor MLA) (paper III). Therefore, by taking advantage of the power density dependence of UCNPs, MLA can quite dramatically enhance the

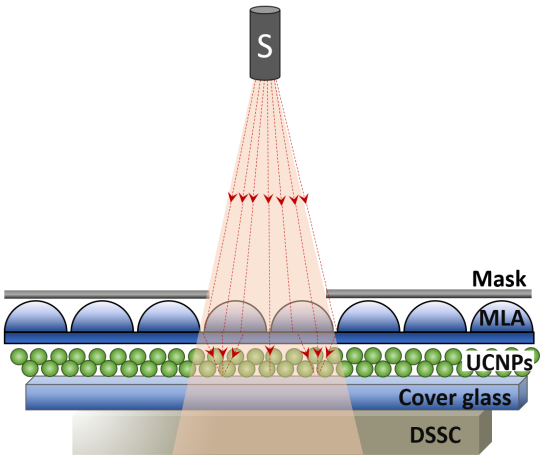

Figure 5.8: *Schematic illustration of UCNP and MLA enhanced DSSC setup.*

UCNPs UCL intensity and further improve the DSSC efficiency. This approach is general and should be possible to combine with other strategies, chemical or optical, for further enhancement of UCL and solar cells efficiency.

5.3.3 UCL enhancement of UCNPs through the plasmonic effect

Plasmonic effect induced UCL enhancement has drawn a large amount of attention for the last ten years.[138,149–154] In general, the UCL intensity is proportional to E^{2n} for a n-photon process, where E is the external electronmagnetic (EM) field. Plasmon resonances on metallic nanostructure surfaces (*e.g.*, Au/Ag nanoparticles) can significantly enhance the EM field near the emitter when the UC emitter is put in a close distance to the metallic nanostructure. There are mainly three ways how the plasmonic effect can affect the UCL emitter center. First of all, due to the enhanced EM field, the absorption and scattering of the UCNPs of the incident light is enhanced, which leads to a bigger absorption cross-section of the sensitizer. Second, the EM field increases the decay speed of the UCL state, radiatively and nonradiatively. Nonradiative decay leads to enhanced quenching and temperature increase, and decreases the UCL intensity, whereas the radiative decay of the UCL state enhances the UCL intensity. Therefore, the competition between radiative and nonradiative enhancement together determines the final enhanced UCL intensity. Thirdly, the EM field also increases the decay speed of the intermediate states, which would decrease the UCL intensity. Therefore, the overall UCL enhancement is determined by all the three processes. The design of UCL enhancement to modify the three influencing factors critically focusses on polarization, antenna material,

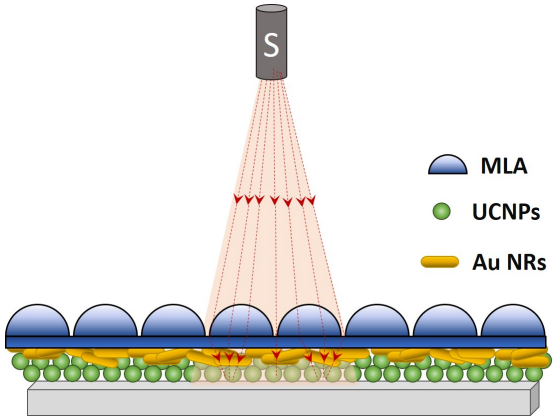

Figure 5.9: *Schematic illustration of UCNP, MLA and Au NRs enhanced UCL intensity configuration.*

morphology control of the antenna material, spectral overlap between the resonances and the absorption/emission wavelength, distance between UCL emitter and antenna material, and pump power.[149] Among them, morphology control is a most flexible and well investigated design strategy. Depending on the geometry of the antenna material, the UCL enhancement factor changes within the range of 1 to over-1000 times.[137,150] Geometries like core-shell,[155] nanoplates,[156] nanorod decoration,[157] sphere assembly,[71,117,158] island films,[159,160] porous film,[161] pillar arrays,[162,163] aperture arrays[164] and nanohole arrays[165] have been applied. Still, many more opportunities for exploration remain for better plasmonic effects for enhancement of the PL.

5.3.4 UCL enhancement through cascade amplification of plasmonic effect&MLA

Even though plasmonic effects can enhance the UCL, still it is difficult to achieve a high UCL enhancement as precise and complicated modifications are needed. A new and easier strategy is to combine the superlensing effect of MLAs and the plasmonic effect together as a cascade amplification of the photon upconversion as shown in Fig. 5.9.

To combine the excellent spatial light modification of MLAs and plasmonic effects of metallic structures, the PL intensity can be enhanced more than four orders of magnitude under weak light excitation (paper IV), with the plasmonic effect enhancing UCL by one order of magnitude and the superlensing effect enhancing UCL by two or three orders of magnitude. This routine is relatively easy to be obtained compared to a pure plasmonic effect enhancement through experimental modification.

Chapter 6

Summary of Included Papers

Paper I

Change in the emission saturation and kinetics of upconversion nanoparticles under different light irradiations.

Niusha Bagheri, **Qingyun Liu**, Jan Bergstrand, Rui Pu, Qiuqiang Zhan, Mohammad Hossein Majles Ara, Hans Ågren, Haichun Liu, Jerker Widengren.

This work concerned upconversion nanoparticles (UCNPs) co-sensitized by both Nd^{3+} and Yb^{3+} with Er^{3+} as emitter that can be excited by both 808 nm and 980 nm excitation, which is beneficial to broaden the absorption range and to enhance the UCL intensity for deep tissue bioimaging. Due to the extra energy transfer step between $Nd^{3+} \rightarrow Yb^{3+}$ and cross relaxation between Nd^{3+} and Er^{3+}, the UCNPs were shown to exhibit different temporal response under 808 nm excitation compared to under 980 nm. With increasing power intensity, the upconversion luminenscence intensity (UCL) is weaker and reaches saturation faster under 808 nm than under 980 nm excitation. What's more, these system exhibited a delayed UCL time correlated intensity profile under 808 nm than 980 nm excitation. These differences are relevant for UCNP related applications like optical encoding and bioimaging, and to explore the kinetics and color tunability. With laser-scanning microscopy, the dwelling time dependence of selective colour readouts was explored as providing a new strategy for multi-wavelength excitation colour display.

I performed most of the experiments, analyzed the data and contributed to the writing of the manuscript.

Paper II

On the decay time of upconversion luminescence.

Jan Bergstrand, **Qingyun Liu**, Bingru Huang, Xingyun Peng, Christian Wurth, Ute Resch-Genger, Qiuqiang Zhan, Jerker Widengren, Hans Ågren and Haichun Liu.

Despite the well developed nanochemistry and applications of UCNPs, there is still a lack of comprehensive studies of upconversion kinetics. This motivated me, in this work, to study the kinetics of upconversion under both anti-Stokes excitation and Stokes excitation methods through numerical simulations based on a rate equation model. A representative standard two-photon upconversion model is applied for the simulation. The results show that factors of sensitizer lifetime, activator intermediate state lifetime and cross relaxation (CR) process affect the decay profile of the UCL emitting state all together under anti-Stokes excitation. Therefore, the extracted decay constant from the UCL decay profile should be regarded as the comprehensive temporal response of the whole UC system to the function of excitation instead of the intrinsic lifetime. Stokes excitation is usually preferred to precisely obtain the intrinsic lifetime of the UCL emitting state, while, the characterization can be invalid when a strong cross relaxation (CR) process is involved. What's more, a strong CR process can also contribute to the power dependence of the UCL.

I contributed to the simulations and data analysis.

Paper III

Microlens array enhanced upconversion luminescence at low excitation irradiance.

Qingyun Liu, Haichun Liu, Deyang Li, Wen Qiao, Guanying Chen and Hans Ågren.

Due to the power dependence of upconversion luminescence (UCL) intensity, the low UCL intensity at mild excitation irradiance hinders applications for photovoltaic devices. Therefore, in this work, a polymeric microlens array (MLA) is applied to spatially modify the light distribution to enhance the UCL efficiency, taking advantage of the nonlinear power dependence of the quantum yield (QY). The experimental results proved their ability to enhance the UCL by more than one order of magnitude under either 980 nm and 808 nm excitation, with more than 225-fold enhancement factor (the 450 nm emission band of Tm^{3+}) at low excitation irradiance. Through theoretical ray tracing simulations, the enhancement ability of MLAs was investigated and varied for different UCL emitting hands (409 nm, 525/540 nm and 654 nm of Er^{3+}) due to different multi-photon processes. The setup of MLAs together with UCNP equipped dye sensitized solar cells was

explored and exhibited an overall 9.51% efficiency enhancement over the control cell.

I performed all the experiments and analyzed the data and contributed to the writing of manuscript.

Paper IV

Cascade photon upconversion amplification for selective multispectral narrow-band near-infrared photodetection.

Yanan Ji, Wen Xu, Nan Ding, Haitao Yang, Hongwei Song, **Qingyun Liu**, Hans Ågren, Jerker Widengren, Haichun Liu.

The fact that it still remains a challenge to detect narrow bands within the NIR range with low visible light noise, motivated me to take part in the development of a NIR photodetector (PD) composed of UCNPs and a perovskite film. By coupling the light spatial modification ability of dielectric microlens arrays (MLAs) with the plasmonic effect of gold nanorods, the upconversion luminescent intensity could be amplified more than four orders of magnitude. Taking advantage of the core-shell-shell structure, multiple ions were doped in physically separated layers and the attenuated PD of the UCNPs was obtained for multi-band detection with the high responsivity of 30.73, 23.15, 12.20 AW^{-1} and detectivity of 5.36, 3.45, 27 1.91×10^{11} Jones for the 808, 980, and 1540 nm light detection, respectively, and with the short response time of 80-120 ms. For the first time I could explore the ability of separating excitations of PDs by taking advantage of the UCL excitation frequency response.

I contributed to the light field simulations and discussion on the results.

Paper V

High throughput decoding approach for luminescence kinetics-based optical encoding of lanthanide upconversion nanoparticles.

Qingyun Liu, Lucía Labrador-Páez, Jan Bergstrand, Xiang Zheng, Yong Zhang, Jerker Widengren, Haichun Liu, Hans Ågren.

For secured data transmission or counterfeiting, optical encoding has become a very popular method fulfilling the demands of rapid data transfer. In this work, we proposed a new optical encoding dimension, namely the pulse duration response of UCNPs. The green emission pulse width response of 525 nm/540 nm of Er^{3+} was characterized by standard equation models for two-photon upconversion rates. A correlation between the averaged UCL *vs* pulse duration profile was obtained both theoretically, through numerical simulation and analytical deduction of rate equations, and experimentally. After excited by a pulsed excitation with fixed duty

cycle and varied pulse duration, the UCL photons were monitored and digitalized by a CCD camera. Through fitting the experimental averaged UCL *vs* pulse duration profiles with theoretical model, time constants of the UCL state and the intermediate state and sensitizer effective lifetime could be extracted as decoding factors to identify the materials. By using this method to encode and decode, it was shown that the data transferred could give high security with a large data storage capacity.

I performed all the experiments and analyzed the data and wrote the manuscript.

Chapter 7

Outlook

The discussion and results in thesis indicate that the kinetics of UCNPs can be well investigated through rate equations models. Due to the sensitivity to parameters of numerical simulations, rather strict conditions are needed for simulations when applied to large upconversion systems. Experiments should be repeated several times and applying more characterization is then helpful to obtain more information to verify the validity of the simulations. Thus feedback and validation between simulations and experiment is important to evaluate the obtained results from the chosen model.

Applying microlens arrays for enhancing upconversion UCL is proven to be far more efficient than using the plasmonic effect of metallic nanoparticles, something that motivates further studies of microlenses with varying size, shape and configuration. The size could be modified to the scale of hundreds of nanometers. One step further, to overcome the light refraction limit when the size of the microlens is below half of the excitation wavlength, some advanced types of optics can be applied, *e.g.*, metasurfaces, to replace traditional optics. The idea of covering each individual UCNP with a metasurface would be a challenging and interesting project to be investigated further.

As reviewed above, optical encoding dimensions have been well developed for optical encoding purpose, and it may, because of this reason, be challenging to develop new encoding dimensions further. Instead, more effort could be put to improve the precision of the encoding and decoding processes. For example, for lifetime encoding&decoding, the lifetime differences affect the precision of optical encoding. With higher accuracy, more lifetime values can be applied and would lead to better statistics and to an increase of the optical encoding capacity.

Last but not the least, for photovoltaic device applications, the gained efficiency from UCNPs is still relatively low. In order to make it work more efficiently,

several strategies could be combined all together: plasmonic effect to enhance absorption, microlens array to enhance the QY and other strategies to enhance doping concentration without reducing the UCL, like applying core-shell hierarchy architecture structures. Dye functionalization of UCNPs, taking advantage of high triplet state density of dyes, is proven to be a way to enhance the PL by five orders of magnitude. Therefore, combining dye antennas of high photostability with MLAs could be an efficient strategy as well. Still, the narrow absorption of UCNPs is a big drawback for solar cell sensitization. Even with multi-sensitizer doping strategies and utilizing advanced core-shell hierarchy architectures, the absorption broadening is limited. If the activator cross absorption can be enhanced significantly, the absorption range can be broadened even more.

These are just a few examples for future lines of development of UCNP research and technology. In my mind, the area is still much in its infancy and holds much promise for future breakthroughs with novel applications which we even cannot imagine today. It is my hope that my thesis work has made a footprint and could serve as inspiration for other researchers to gain further knowledge, understanding and know-how of these fantastic lanthanide upconversion systems, not just to find new applications but also to satisfy our curiosity.

REFERENCES

[1]G. Shavi, P. Deshpande, U. Nayak, A. K. Gurram, R. K. Averineni, M. Reddy, N. Udupa, and K. Koteshwara, International Journal of Green Nanotechnology: Biomedicine, **2**, B67–B81, 12 2010.

[2]C. Yuan, L. Li, J. Huang, Z. Ning, L. Sun, and H. Ågren, Nanomaterials, **6**(6), 97, May 2016.

[3]N. Toshima, Macromolecular Symposia, **270**(1), 27–39, 2008.

[4]C. Tablero, **106**(7), 074306, 2009.

[5]Y. Tang, X. Zeng, and J. Liang, J Chem Educ, **87**(7), 742–746, 2010.

[6]S. Mehrabani and A. M. Armani, Opt. Lett., **38**(21), 4346–4349, Nov 2013.

[7]H. D. Chen, S. M. Lee, A. Montenegro, D. Kang, B. J. Gai, H. Lim, C. Dutta, W. T. He, M. L. Lee, A. Benderskii, and J. Yoon, Acs Photonics, **5**(11), 4289–4295, 2018.

[8]Q. Tian, W. Yao, W. Wu, and C. Jiang, Nanoscale Horiz., **4**, 10–25, 2019.

[9]L. He, L. Yang, H. Zhu, W. Dong, Y. Ding, and J. J. Zhu, Methods and Applications in Fluorescence, **5**(2), 024010, may 2017.

[10]J. Lee, B. Yoo, H. Lee, G. D. Cha, H. S. Lee, Y. Cho, S. Y. Kim, H. Seo, W. Lee, D. Son, M. Kang, H. M. Kim, Y. I. Park, T. Hyeon, and D. H. Kim, Advanced Materials, **29**(1), 2017.

[11]F. Wang, D. Banerjee, Y. Liu, X. Chen, and X. Liu, Analyst, **135**, 1839–1854, 2010.

[12]F. Wang and X. Liu, Chem. Soc. Rev., **38**, 976–989, 2009.

[13]G. Y. Chen, H. Agren, T. Y. Ohulchanskyy, and P. N. Prasad, Chemical Society Reviews, **44**(6), 1680–1713, 2015.

[14]R. Rafique, S. H. Baek, C. Y. Park, S. J. Chang, A. R. Gul, S. Ha, T. P. Nguyen, H. Oh, S. Ham, M. Arshad, H. Lee, and T. J. Park, Scientific Reports, **8**(1), 17101, 2018.

[15]J. Zhou, Y. Sun, X. X. Du, L. Q. Xiong, H. Hu, and F. Y. Li, Biomaterials, **31**(12), 3287–3295, 2010.

[16]W. J. Yao, Q. Y. Tian, B. Tian, M. X. Li, H. J. Wang, P. Zeng, L. Liu, H. Zheng, and W. Wu, Science China-Materials, **62**(3), 368–378, 2019.

[17]C. Z. Yuan, G. Y. Chen, L. Li, J. A. Damasco, Z. J. Ning, H. Xing, T. M. Zhang, L. C. Sun, H. Zeng, A. N. Cartwright, P. N. Prasad, and H. Agren, Acs Applied Materials & Interfaces, **6**(20), 18018–18025, 2014.

[18]C. Z. Yuan, G. Y. Chen, P. N. Prasad, T. Y. Ohulchanskyy, Z. J. Ning, H. N. Tian, L. C. Sun, and H. Agren, Journal of Materials Chemistry, **22**(33), 16709–16713, 2012.

[19]J. C. G. Bünzli, Journal of Coordination Chemistry, **67**(23-24), 3706–3733, 2014.

[20]F. F. V.A.G. Rivera and E. M. Jr. *Localized Surface Plasmon Resonances: Noble Metal Nanoparticle Interaction with Rare-Earth Ions.* Plasmonics: principles and applications. IntechOpen, 2012.

[21]A. J. Freeman and R. E. Watson, Phys. Rev., **127**, 2058–2075, Sep 1962.

[22]H. Li, M. L. Tan, X. Wang, F. Li, Y. Q. Zhang, L. L. Zhao, C. H. Yang, and G. Y. Chen, Journal of the American Chemical Society, **142**(4a), 2023–2030, 2020.

[23]A. F. Garcia-Flores, J. S. Matias, D. J. Garcia, E. D. Martinez, P. S. Cornaglia, G. G. Lesseux, R. A. Ribeiro, R. R. Urbano, and C. Rettori, Physical Review B, **96**(16), 2017.

[24]W. J. Kong, J. Shan, and Y. G. Ju, Materials Letters, **64**(6), 688–691, 2010.

[25]G. Chen, H. Qiu, P. N. Prasad, and X. Chen, Chem Rev, **114**(10), 5161–214, 2014.

[26]D. M. Yang, Y. L. Dai, J. H. Liu, Y. Zhou, Y. Y. Chen, C. X. Li, P. A. Ma, and J. Lin, Biomaterials, **35**(6), 2011–2023, 2014.

[27]X. D. Wang and G. Y. Chen, Frontiers in Chemistry, **7**, 2019.

[28]A. Sarakovskis, M. Voss, G. Doke, D. Jankovica, and J. Grube, International Conference on Functional Materials and Nanotechnologies (Fm & Nt2012), **38**, 2012.

[29]X. Chen, D. F. Peng, Q. Ju, and F. Wang, Chemical Society Reviews, **44**(6), 1318–1330, 2015.

[30]M. Kaiser, C. Würth, M. Kraft, T. Soukka, and U. Resch-Genger, Nano Research, **12**(8), 1871–1879, 2019.

[31]X. Chen, D. F. Peng, Q. Ju, and F. Wang, Chemical Society Reviews, **44**(6), 1318–1330, 2015.

[32]G. S. Yi and G. M. Chow, Chemistry of Materials, **19**(3), 341–343, 2007.

[33]H. X. Mai, Y. W. Zhang, L. D. Sun, and C. H. Yan, Journal of Physical Chemistry C, **111**(37), 13721–13729, 2007.

[34]Y. Wang, L. P. Tu, J. W. Zhao, Y. J. Sun, X. G. Kong, and H. Zhang, Journal of Physical Chemistry C, **113**(17), 7164–7169, 2009.

[35]N. J. J. Johnson, A. Korinek, C. H. Dong, and F. C. J. M. van Veggel, Journal of the American Chemical Society, **134**(27), 11068–11071, 2012.

[36]J. C. Boyer, M. P. Manseau, J. I. Murray, and F. C. J. M. van Veggel, Langmuir, **26**(2), 1157–1164, 2010.

[37]J. C. Boyer and F. C. J. M. van Veggel, Nanoscale, **2**(8), 1417–1419, 2010.

[38]M. L. Chen, Y. Ma, and M. Y. Li, Materials Letters, **114**, 80–83, 2014.

[39]Q. H. Zeng, B. Xue, Y. L. Zhang, D. Wang, X. M. Liu, L. P. Tu, H. F. Zhao, X. G. Kong, and H. Zhang, Crystengcomm, **15**(23), 4765–4772, 2013.

[40]L. Lei, D. Q. Chen, W. J. Zhu, J. Xu, and Y. S. Wang, Chemistry-an Asian Journal, **9**(10), 2765–2770, 2014.

[41]B. Zhou, L. Tao, Y. H. Tsang, and W. Jin, Journal of Materials Chemistry C, **1**(28), 4313–4318, 2013.

[42]H. L. Qiu, C. H. Yang, W. Shao, J. Damasco, X. L. Wang, H. Agren, P. N. Prasad, and G. Y. Chen, Nanomaterials, **4**(1), 55–68, 2014.

[43]Y. T. Zhong, G. Tian, Z. J. Gu, Y. J. Yang, L. Gu, Y. L. Zhao, Y. Ma, and J. N. Yao, Advanced Materials, **26**(18), 2831–2837, 2014.

[44]X. M. Li, Z. Z. Guo, T. C. Zhao, Y. Lu, L. Zhou, D. Y. Zhao, and F. Zhang, Angewandte Chemie-International Edition, **55**(7), 2464–2469, 2016.

[45]B. R. Huang, Q. S. Wu, X. Y. Peng, L. Q. Yao, D. F. Peng, and Q. Q. Zhan, Nanoscale, **10**(45), 21025–21030, 2018.

[46]P. Y. Wang, X. M. Li, C. Yao, W. X. Wang, M. Y. Zhao, A. M. El Toni, and F. Zhang, Biomaterials, **125**, 90–100, 2017.

[47]J. P. Lai, Y. X. Zhang, N. Pasquale, and K. B. Lee, Angewandte Chemie-International Edition, **53**(52), 14419–14423, 2014.

[48]H. L. Wen, H. Zhu, X. Chen, T. F. Hung, B. L. Wang, G. Y. Zhu, S. F. Yu, and F. Wang, Angewandte Chemie-International Edition, **52**(50), 13419–13423, 2013.

[49]H. U. Gudel and M. Pollnau, Journal of Alloys and Compounds, **303**, 307–315, 2000.

[50]F. Auzel, Chemical Reviews, **104**(1), 139–173, 2004.

[51]R. M. Clegg. Chapter 1 förster resonance energy transfer—fret what is it, why do it, and how it's done. In *Fret and Flim Techniques*, volume 33 of *Laboratory Techniques in Biochemistry and Molecular Biology*, pages 1 – 57. Elsevier, 2009.

[52]D. L. Dexter, The Journal of Chemical Physics, **21**(5), 836–850, 1953.

[53]S. D. Jackson, Optics Communications, **230**, 197–203, Jan 2004.

[54]V.Lavín, F.Lahoz, I.R.Martín, U.R.Rodríguez-Mendoza, and J.M.Cáceres, Optical Materials, **27**(11), 1754–1761, Oct 2005.

[55]J. F. Suyver, A. Aebischer, S. Garcia-Revilla, P. Gerner, and H. U. Gudel, Physical Review B, **71**(12), 2005.

[56]M. Pollnau, D. R. Gamelin, S. R. Luthi, H. U. Gudel, and M. P. Hehlen, Physical Review B, **61**(5), 3337–3346, 2000.

[57]L. M. Jin, X. Chen, C. K. Siu, F. Wang, and S. F. Yu, Acs Nano, **11**(1), 843–849, 2017.

[58]H. Liu, C. T. Xu, G. Dumlupinar, O. B. Jensen, P. E. Andersen, and S. Andersson-Engels, Nanoscale, **5**(20), 10034–40, 2013.

[59]H. C. Liu, C. T. Xu, G. Dumlupinar, O. B. Jensen, P. E. Andersen, and S. Andersson-Engels, Nanoscale, **5**(20), 10034–10040, 2013.

[60]A. Bansal, H. C. Liu, M. K. G. Jayakumar, S. Andersson-Engels, and Y. Zhang, Small, **12**(13), 1732–1743, 2016.

[61]M. Wang, G. Abbineni, A. Clevenger, C. B. Mao, and S. K. Xu, Nanomedicine-Nanotechnology Biology and Medicine, **7**(6), 710–729, 2011.

[62]S. S. Cui, H. Y. Chen, and Y. Q. Gu, 9th International Conference on Photonics and Imaging in Biology and Medicine (Pibm 2010), **277**, 2011.

[63]X. Liang, X. Wang, J. Zhuang, Q. Peng, and Y. Li, Inorganic Chemistry, **46**(15), 6050–6055, 2007.

[64]R. Rafique, S. H. Baek, L. M. T. Phan, S. J. Chang, A. R. Gul, and T. J. Park, Materials Science & Engineering C-Materials for Biological Applications, **99**, 1067–1074, 2019.

[65]M. Wang, Y. Zhu, and C. Mao, Langmuir, **31**(25), 7084–7090, 2015.

[66]M. Wang, J. L. Liu, Y. X. Zhang, W. Hou, X. L. Wu, and S. K. Xu, Materials Letters, **63**(2), 325–327, 2009.

[67]Z. Li and Y. Zhang, Angewandte Chemie International Edition, **45**(46), 7732–7735, 2006.

[68]A. Dong, X. Ye, J. Chen, Y. Kang, T. Gordon, J. M. Kikkawa, and C. B. Murray, Journal of the American Chemical Society, **133**(4), 998–1006, 2011.

[69]G. Yi and G. Chow, Advanced Functional Materials, **16**(18), 2324–2329, 2006.

[70]M. Kaiser, C. Wurth, M. Kraft, I. Hyppanen, T. Soukka, and U. Resch-Genger, Nanoscale, **9**(28), 10051–10058, 2017.

[71]C. T. Xu, P. Svenmarker, H. C. Liu, X. Wu, M. E. Messing, L. R. Wallenberg, and S. Andersson-Engels, Acs Nano, **6**(6), 4788–4795, 2012.

[72]M. Y. Hossan, A. Hor, Q. Luu, S. J. Smith, P. S. May, and M. T. Berry, Journal of Physical Chemistry C, **121**(30), 16592–16606, 2017.

[73]H. C. Liu, C. T. Xu, D. Lindgren, H. Y. Xie, D. Thomas, C. Gundlach, and S. Andersson-Engels, Nanoscale, **5**(11), 4770–4775, 2013.

[74]M. Gonzalez-Bejar, L. Frances-Soriano, and J. Perez-Prieto, Frontiers in Bioengineering and Biotechnology, **4**, 2016.

[75]X. Ai, J. Aw, and B. Xing. *Upconversion Nanoparticles for Bioimaging*, pages 363–390. Springer Singapore, Singapore, 2016.

[76]M. Nyk, R. Kumar, T. Y. Ohulchanskyy, E. J. Bergey, and P. N. Prasad, Nano Letters, **8**(11), 3834–3838, 2008.

[77]Z. J. Li, Y. W. Zhang, H. E. La, R. Zhu, G. El-Banna, Y. Z. Wei, and G. Han, Nanomaterials, **5**(4), 2148–2168, 2015.

[78]E. Hemmer, N. Venkatachalam, H. Hyodo, A. Hattori, Y. Ebina, H. Kishimoto, and K. Soga, Nanoscale, **5**(23), 11339–11361, 2013.

[79]A. Xia, M. Chen, Y. Gao, D. M. Wu, W. Feng, and F. Y. Li, Biomaterials, **33**(21), 5394–5405, 2012.

[80]G. Y. Chen, J. Shen, T. Y. Ohulchanskyy, N. J. Patel, A. Kutikov, Z. P. Li, J. Song, R. K. Pandey, H. Agren, P. N. Prasad, and G. Han, Acs Nano, **6**(9), 8280–8287, 2012.

[81]J. Park, K. Kim, E. J. Jo, W. Kim, H. Kim, R. Lee, J. Y. Lee, J. Y. Jo, M. G. Kim, and G. Y. Jung, Nanoscale, **11**(47), 22813–22819, 2019.

[82]D. Gamelin and H. Gudel. *Upconversion Processes in Transition Metal and Rare Earth Metal Systems*, volume 214, pages 1–56. 01 2001.

[83]K. Huang, N. M. Idris, and Y. Zhang, Small, **12**(7), 836–852, 2016.

[84]W. P. Qin, C. Y. Cao, L. L. Wang, J. S. Zhang, D. S. Zhang, K. Z. Zheng, Y. Wang, G. D. Wei, G. F. Wang, P. F. Zhu, and R. Kim, Optics Letters, **33**(19), 2167–2169, 2008.

[85]F. Wang and X. G. Liu, Journal of the American Chemical Society, **130**(17), 5642–+, 2008.

[86]H. H. Gorris, R. Ali, S. M. Saleh, and O. S. Wolfbeis, Advanced Materials, **23**(14), 1652–+, 2011.

[87]L. Zhou, Y. Fan, R. Wang, X. M. Li, L. L. Fan, and F. Zhang, Angewandte Chemie-International Edition, **57**(39), 12824–12829, 2018.

[88]K. Hoffmann, T. Behnke, D. Drescher, J. Kneipp, and U. Resch-Genger, Acs Nano, **7**(8), 6674–6684, 2013.

[89]H. C. Liu, M. K. G. Jayakumar, K. Huang, Z. Wang, X. Zheng, H. Agren, and Y. Zhang, Nanoscale, **9**(4), 1676–1686, 2017.

[90]X. W. Liu, Y. Wang, X. Y. Li, Z. G. Yi, R. R. Deng, L. L. Liang, X. J. Xie, D. T. B. Loong, S. Y. Song, D. Y. Fan, A. H. All, H. J. Zhang, L. Huang, and X. G. Liu, Nature Communications, **8**, 2017.

[91]C. F. Guo, T. Y. Sun, F. Cao, Q. Liu, and Z. F. Ren, Light-Science & Applications, **3**, 2014.

[92]C. Xie, P. You, Z. K. Liu, L. Li, and F. Yan, Light-Science & Applications, **6**, 2017.

[93]H. C. Liu, K. Huang, R. R. Valiev, Q. Q. Zhan, Y. Zhang, and H. Agren, Laser & Photonics Reviews, **12**(1), 2018.

[94]K. C. Liu, Z. Y. Zhang, C. X. Shan, Z. Q. Feng, J. S. Li, C. L. Song, Y. N. Bao, X. H. Qi, and B. Dong, Light-Science & Applications, **5**, 2016.

[95]F. Wang, S. H. Wen, H. He, B. M. Wang, Z. G. Zhou, O. Shimoni, and D. Y. Jin, Light-Science & Applications, **7**, 2018.

[96]R. R. Deng, F. Qin, R. F. Chen, W. Huang, M. H. Hong, and X. G. Liu, Nature Nanotechnology, **10**(3), 237–242, 2015.

[97]W. P. Qin, Z. Y. Liu, C. N. Sin, C. F. Wu, G. S. Qin, Z. Chen, and K. Z. Zheng, Light-Science & Applications, **3**, 2014.

[98]C. Yuan, G. Chen, L. Li, J. A. Damasco, Z. Ning, H. Xing, T. Zhang, L. Sun, H. Zeng, A. N. Cartwright, P. N. Prasad, and H. Ågren, ACS Applied Materials & Interfaces, **6**(20), 18018–18025, 2014. PMID: 25238319.

[99]C. Yuan, G. Chen, P. N. Prasad, T. Y. Ohulchanskyy, Z. Ning, H. Tian, L. Sun, and H. Ågren, Journal of Materials Chemistry, **22**(33), 16709–16713, 2012.

[100]S. W. Hao, Y. F. Shang, D. Y. Li, H. Agren, C. H. Yang, and G. Y. Chen, Nanoscale, **9**(20), 6711–6715, 2017.

[101]D. W. Lu, C. C. Mao, S. K. Cho, S. Ahn, and W. Park, Scientific Reports, **6**, 2016.

[102]Y. Liu, T. Sun, W. L. Ma, W. Z. Yu, S. B. Nanjunda, S. J. Li, and Q. L. Bao, Chinese Optics Letters, **16**(2), 2018.

[103]R. Saran and R. J. Curry, Nature Photonics, **10**(2), 81–92, 2016.

[104]F. B. Huang, Y. Li, H. Q. Xia, J. P. Zhang, K. Xu, Y. Q. Peng, and G. H. Liu, Carbon, **118**, 666–674, 2017.

[105]J. D. Yao, Z. Q. Zheng, and G. W. Yang, Advanced Functional Materials, **27**(33), 2017.

[106]F. B. Huang, Y. Li, H. Q. Xia, J. P. Zhang, K. Xu, Y. Q. Peng, and G. H. Liu, Carbon, **118**, 666–674, 2017.

[107]S. Chen, C. J. Teng, M. Zhang, Y. R. Li, D. Xie, and G. Q. Shi, Advanced Materials, **28**(28), 5969–+, 2016.

[108]H. T. Yuan, X. G. Liu, F. Afshinmanesh, W. Li, G. Xu, J. Sun, B. Lian, A. G. Curto, G. J. Ye, Y. Hikita, Z. X. Shen, S. C. Zhang, X. H. Chen, M. Brongersma, H. Y. Hwang, and Y. Cui, Nature Nanotechnology, **10**(8), 707–713, 2015.

[109]J. Kaniewski and J. Piotrowski, Opto-electronics Review, **12**, 03 2004.

[110]M. Kataria, K. Yadav, S. Y. Cai, Y. M. Liao, H. I. Lin, T. L. Shen, Y. H. Chen, Y. T. Chen, W. H. Wang, and Y. F. Chen, Acs Nano, **12**(9), 9596–9607, 2018.

[111]M. K. Thakur, A. Gupta, M. Y. Fakhri, R. S. Chen, C. T. Wu, K. H. Lin, and S. Chattopadhyay, Nanoscale, **11**(19), 9716–9725, 2019.

[112]Y. W. Zhang, J. Wang, B. Wang, J. H. Shao, J. A. Deng, C. X. Cong, L. G. Hu, P. F. Tian, R. Liu, S. L. Zhang, and Z. J. Qiu, Advanced Optical Materials, **6**(21), 2018.

[113]J. H. Wu, Z. W. Yang, C. Y. Qiu, Y. J. Zhang, Z. Q. Wu, J. L. Yang, Y. H. Lu, J. F. Li, D. X. Yang, R. Hao, E. P. Li, G. L. Yu, and S. S. Lin, Nanoscale, **10**(17), 8023–8030, 2018.

[114]S. Ghosh, W. C. Chiang, M. Y. Fakhri, C. T. Wu, R. S. Chen, and S. Chattopadhyay, Nano Energy, **67**, 2020.

[115]J. Christiansen, H. Lakhotiya, E. Eriksen, S. P. Madsen, P. Balling, and B. Julsgaard, Journal of Applied Physics, **125**(4), 043106, 2019.

[116]M. Y. Hossan. *Rate Equations Modeling of Upconversion Dynamics in Er, Yb and Tm, Yb doped β-NaYF4 Nanophosphors.* Thesis, 2019.

[117]S. Schietinger, T. Aichele, H. Q. Wang, T. Nann, and O. Benson, Nano Letters, **10**(1), 134–138, 2010.

[118]C. F. Gainer, G. S. Joshua, C. R. De Silva, and M. Romanowski, Journal of Materials Chemistry, **21**(46), 18530–18533, 2011.

[119]P. Villanueva-Delgado, K. W. Kramer, and R. Valiente, Journal of Physical Chemistry C, **119**(41), 23648–23657, 2015.

[120]S. S. Du, D. Y. Wang, Q. P. Qiang, X. L. Ma, Z. B. Tang, and Y. H. Wang, Journal of Materials Chemistry C, **4**(29), 7148–7155, 2016.

[121]Q. L. Zou, P. Huang, W. Zheng, W. W. You, R. F. Li, D. T. Tu, J. Xu, and X. Y. Chen, Nanoscale, **9**(19), 6521–6528, 2017.

[122]F. W. Ostermayer and L. G. Van Uitert, Physical Review B, **1**(11), 4208–4212, 1970.

[123]G. S. Maciel, A. Biswas, and P. N. Prasad, Optics Communications, **178**(1-3), 65–69, 2000.

[124]T. Miyakawa and D. L. Dexter, Physical Review B, **1**(1), 70–80, 1970.

[125]B. M. Walsh. Judd-ofelt theory: principles and practices. Advances in Spectroscopy for Lasers and Sensing, pages 403–433. Springer Netherlands.

[126]T. Kushida, Journal of the Physical Society of Japan, **34**(5), 1318–1326, 1973.

[127]H. X. Zhang, T. Q. Jia, X. Y. Shang, S. A. Zhang, Z. R. Sun, and J. R. Qiu, Physical Chemistry Chemical Physics, **18**(37), 25905–25914, 2016.

[128]S. LI, M. ZHANG, Y. PENG, Q. ZHANG, and M. ZHAO, Journal of Rare Earths, **28**(2), 237 – 242, 2010.

[129]Y. D. Han, H. Y. Li, Y. B. Wang, Y. Pan, L. Huang, F. Song, and W. Huang, Scientific Reports, **7**, 2017.

[130]M. K. Thakur, A. Gupta, M. Y. Fakhri, R. S. Chen, C. T. Wu, K. H. Lin, and S. Chattopadhyay, Nanoscale, **11**(19), 9716–9725, 2019.

[131]Y. Ji, W. Xu, D. Li, D. Zhou, X. Chen, N. Ding, J. Li, N. Wang, X. Bai, and H. Song, Nano Energy, **61**, 211–220, 2019.

[132]M. Kataria, K. Yadav, G. Haider, Y. M. Liao, Y. R. Liou, S. Y. Cai, H. i. Lin, Y. H. Chen, C. R. Paul Inbaraj, K. P. Bera, H. M. Lee, Y. T. Chen, W. H. Wang, and Y. F. Chen, ACS Photonics, **5**(6), 2336–2347, 2018.

[133]A. Nadort, V. K. A. Sreenivasan, Z. Song, E. A. Grebenik, A. V. Nechaev, V. A. Semchishen, V. Y. Panchenko, and A. V. Zvyagin, Plos One, **8**(5), 2013.

[134]J. H. Zhang, Z. D. Hao, J. Li, X. Zhang, Y. S. Luo, and G. H. Pan, Light-Science & Applications, **4**, 2015.

[135]G. Y. Chen, G. Somesfalean, Y. Liu, Z. G. Zhang, Q. Sun, and F. P. Wang, Physical Review B, **75**(19), 2007.

[136]B. Xue, D. Wang, Y. Zhang, J. Zuo, Y. Chang, T. Langping, X. Liu, Z. Yuan, H. Zhao, J. Song, J. Qu, and X. Kong, Journal of Materials Chemistry C, 2019.

[137]A. Das, C. C. Mao, S. Cho, K. Kim, and W. Park, Nature Communications, **9**, 2018.

[138]R. J. Amjad, M. R. Sahar, S. K. Ghoshal, M. R. Dousti, S. Riaz, A. R. Samavati, M. N. A. Jamaludin, and S. Naseem, Chinese Physics Letters, **30**(2), 2013.

[139]M. D. Wisser, S. Fischer, C. Siefe, A. P. Alivisatos, A. Salleo, and J. A. Dionne, Nano Letters, **18**(4), 2689–2695, 2018.

[140]J. K. Tseng, Y. J. Chen, C. T. Pan, T. T. Wu, and M. H. Chung, Solar Energy, **85**(9), 2167–2178, 2011.

[141]M. Schmid and P. Manley, Journal of Photonics for Energy, **5**(1), 2014.

[142]A. Peer, R. Biswas, J. M. Park, R. Shinar, and J. Shinar, Opt Express, **25**(9), 10704–10709, 2017.

[143]M. Nam, K. Kim, J. Lee, K. K. Lee, and S. S. Yang, Solar Energy, **91**, 374–380, 2013.

[144]Y. Chen, M. Elshobaki, Z. Ye, J. M. Park, M. A. Noack, K. M. Ho, and S. Chaudhary, Phys Chem Chem Phys, **15**(12), 4297–302, 2013.

[145]P. Nussbaum, R. Volke, H. P. Herzig, M. Eisner, and S. Haselbeck, Pure and Applied Optics, **6**(6), 617–636, 1997.

[146]C. Chao and G. D. Su, Current Developments in Lens Design and Optical Engineering Xix, **10745**, 2018.

[147]A. Akatay and H. Urey, Optics Express, **15**(8), 4523–4529, 2007.

[148]B. Zhou, B. Y. Shi, D. Y. Jin, and X. G. Liu, Nature Nanotechnology, **10**(11), 924–936, 2015.

[149]J. Dong, W. Gao, Q. Han, Y. Wang, J. Qi, X. Yan, and M. Sun, Reviews in Physics, **4**, 2019.

[150]D. M. Wu, A. Garcia-Etxarri, A. Salleo, and J. A. Dionne, Journal of Physical Chemistry Letters, **5**(22), 4020–4031, 2014.

[151]Q. C. Sun, H. Mundoor, J. C. Ribot, V. Singh, I. I. Smalyukh, and P. Nagpal, Nano Letters, **14**(1), 101–106, 2014.

[152]S. Fischer, F. Hallermann, T. Eichelkraut, G. von Plessen, K. W. Kramer, D. Biner, H. Steinkemper, M. Hermle, and J. C. Goldschmidt, Optics Express, **20**(1), 271–282, 2012.

[153]S. Fischer, F. Hallermann, T. Eichelkraut, G. von Plessen, K. W. Kramer, D. Biner, H. Steinkemper, M. Hermle, and J. C. Goldschmidt, Optics Express, **21**(9), 10606–10611, 2013.

[154]M. A. Khan and H. Idriss, Wiley Interdisciplinary Reviews-Energy and Environment, **6**(6), 2017.

[155]H. Zhang, Y. J. Li, I. A. Ivanov, Y. Q. Qu, Y. Huang, and X. F. Duan, Angewandte Chemie-International Edition, **49**(16), 2865–2868, 2010.

[156]K. Poorkazem, A. V. Hesketh, and T. L. Kelly, Journal of Physical Chemistry C, **118**(12), 6398–6404, 2014.

[157]P. Kannan, F. A. Rahim, R. Chen, X. Teng, L. Huang, H. D. Sun, and D. H. Kim, Acs Applied Materials & Interfaces, **5**(9), 3508–3513, 2013.

[158]M. Saboktakin, X. C. Ye, S. J. Oh, S. H. Hong, A. T. Fafarman, U. K. Chettiar, N. Engheta, C. B. Murray, and C. R. Kagan, Acs Nano, **6**(10), 8758–8766, 2012.

[159]T. Aisaka, M. Fujii, and S. Hayashi, Applied Physics Letters, **92**(13), 2008.

[160]H. Zhang, D. Xu, Y. Huang, and X. F. Duan, Chemical Communications, **47**(3), 979–981, 2011.

[161]W. Xu, S. Xu, Y. S. Zhu, T. Liu, X. Bai, B. A. Dong, L. Xu, and H. W. Song, Nanoscale, **4**(22), 6971–6973, 2012.

[162]W. H. Zhang, F. Ding, and S. Y. Chou, Advanced Materials, **24**(35), Op236–Op241, 2012.

[163]Q. Luu, A. Hor, J. Fisher, R. B. Anderson, S. Liu, T. S. Luk, H. P. Paudel, M. F. Baroughi, P. S. May, and S. Smith, Journal of Physical Chemistry C, **118**(6), 3251–3257, 2014.

[164]E. Verhagen, L. Kuipers, and A. Polman, Optics Express, **17**(17), 14586–14598, 2009.

[165]M. Saboktakin, X. C. Ye, U. K. Chettiar, N. Engheta, C. B. Murray, and C. R. Kagan, Acs Nano, **7**(8), 7186–7192, 2013.